Supporting Information

Singlet oxygen partition between the outer-, inner- and membrane- phases of photo/chemotherapeutic liposomes.

Vladimir Kabanov,[a] Sanjana Ghosh,[b] Jonathan Lovell[b] and Belinda Heyne[a]*

[a] Department of Chemistry, University of Calgary,
2500 University Drive NW, Calgary, Alberta, Canada, T2N 1N4

[b] Department of Biomedical Engineering, University at Buffalo, Buffalo, NY, 14260, USA

*Email: bjmheyne@ucalgary.ca

Table of Contents:

1. General Procedures

All reagents were purchased from Sigma-Aldrich and used without further purification unless otherwise stated. All water was obtained from a MilliQ Academic A10 ultrapure water purifier working at a resistance of 18.2 MΩ·cm. 99.9% deuterated atom content D_2O was obtained from Sigma-Aldrich. All liposome formulations were stored in their respective buffered solutions at 4 °C until they were used.

1.1 Preparation of the empty and drug-carrying PoP liposomes

Unless noted otherwise, lipids were acquired from Corden Pharma International and other materials were acquired from Sigma Aldrich. Porphyrin phospholipid (PoP) was synthesized as described previously.[1] As reported previously, the formulation for DOX@PoP liposomes included 53 mol. % 1,2-distearoyl-sn-glycero-3-phosphocholine (DSPC, Corden Pharma# LP-R4-076), 40 mol. % cholesterol (PhytoChol, Wilshire Technologies Inc. #57-88-5), 2 mol. % PoP and 5 mol. % 1,2- distearoyl-sn-glycero-3-phosphoethanolamine-N-[methoxy(polyethylene glycol)-2000] (MPEG-2000-DSPE, Corden Pharma# LP-R4-039).[2] To prepare 5 mL (20 mg/mL) of DOX@PoP liposomes, 100 mg of lipids as per the mentioned ratio was dissolved in 1 mL ethanol at 60 °C and then 4 mL of 250 mM ammonium sulfate (pH 5.5) was injected into the lipid mixture. The lipid mixture was then extruded 10 times at 60-70 ° C through sequentially stacked polycarbonate membranes of 0.2, 0.1 and 0.08 µm pore size in a high pressure nitrogen extruder (Northern lipids), followed by dialysis (at least twice) in 800 mL solution of 10% sucrose with 10 mM Histidine (pH 6.5) buffer to remove free ammonium sulfate. Doxorubicin (Dox LC Labs # D-4000) was loaded in the liposomes by incubating Dox in PoP liposomes at 60 °C for 1 hour in Dox:lipid loading molar ratio of 1:5. To generate PoP liposomes loaded with Irinotecan, a method was developed by modifying a formulation reported before.[3] For a 5 mL batch (20 mg/mL), the liposomes were prepared by injecting 1 mL ethanol at 60 °C into the lipids (DSPC: Chol: PoP: MPEG-2000-DSPE in molar ratio of 58.7:40:1:0.3), followed by adding 4 mL of 120 mM ammonium sucrose octasulfate at 60 °C. The lipid mixture was then passed 10 times through a high-pressure nitrogen extruder (Northern lipids) having sequentially stacked polycarbonate membranes of 0.2, 0.1 and 0.08 µm pore size. To remove free ammonium sucrose octasulfate, dialysis of the liposomes was done in 800 mL solution of 145 mM sodium chloride with 5mM HEPES (pH 6.5) changing the buffer at least twice. Irinotecan (Irinotecan, LC Labs # I4122) was loaded in the liposomes by adding drug to liposomes in drug:lipids molar ratio of 1:8 at 60 ° for 1 hour. In all cases, drug loading was greater than 90 %.

1.2 Preparation of the reference PNN@EGG liposomes

Perinaphthenone (PNN) carrying liposomes were prepared in order to serve the role of a reference photosensitizer in the quantification of the quantum yield of singlet oxygen production via direct singlet oxygen phosphorescence detection method. First, 4 mg of PNN was dissolved in 1 mL of reagent grade chloroform. Next, in a 50 mL round bottom flask, a 70 µL aliquot (~1.5 µmol) of the PNN stock was diluted in 3mL of chloroform solution containing 25 mg of L-α-Phosphatidylcholine (Egg. Chicken) lipids provided by Avanti Polar Lipids. The mixture was mixed well before the solvent was removed on a rotary evaporator allowing the lipid-dye contents to form a uniform film on the flask walls. After complete solvent removal,

5 mL of 0.1 M phosphate-buffered silane (pH = 7.4) solution was added to the lipid-dye film and the contents of the flask were agitated via sonication. Murky yellow solution was then extruded at high pressure through a 100 nm porous membrane. The extrusion was performed 10 times in sequence to ensure uniform size distribution of the resulting lipid vesicles. The resulting PNN@EGG liposomes were characterized via dynamic light scattering measurements which revealed uniform liposome size distribution with a mean diameter of 102 nm (Figure S1).

2. Physical Characterization

2.1 Dynamic light scattering and Zeta Potential

Dynamic light scattering and zeta potential measurements (section 3.5) were obtained using Zetasizer Nano (Malvern) instrument (λ_{ex} = 640 nm). All measurements were performed on dilute liposome samples in H_2O, or in 95% D_2O, at a concentration such that the optical density of the samples at the excitation wavelength (640 nm) was below 0.05.

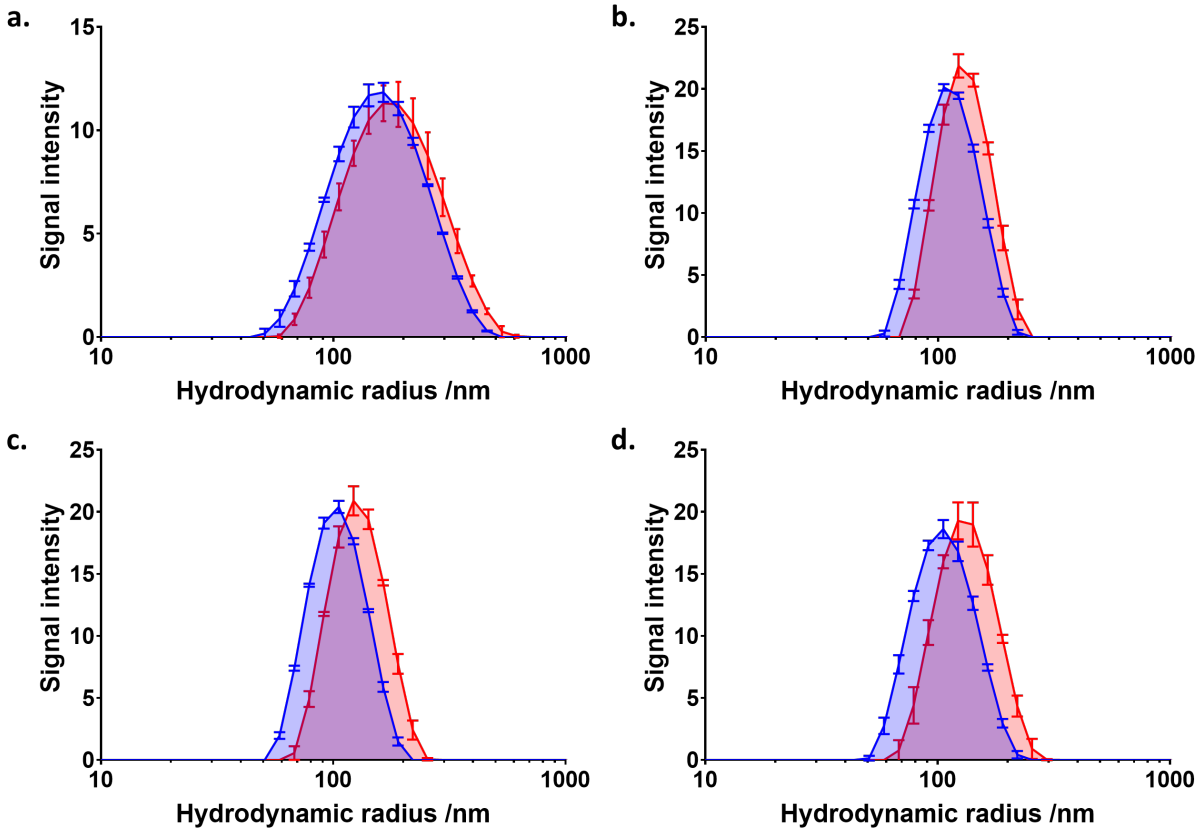

Figure S1: Size distribution of (a.) Empty PoP liposomes: Z-average size in H_2O = 167 nm, in 95% D_2O = 180 nm; (b.) DOX@PoP liposomes: Z-average size in H_2O = 100 nm, in 95% D_2O = 123; (c.) IRT@PoP liposomes: Z-average size in H_2O = 110 nm, in 95% D_2O = 131; (d.) PNN@EGG liposomes: Z-average size in H_2O = 102 nm, in 95% D_2O = 127. Data shown in blue is for samples in H_2O, in red is for samples in 95% D_2O. Error bars represent standard deviation between duplicate measurements.

3. Photophysical Characterization

3.1 UV-Visible and fluorescence emission spectra

UV-Vis absorption spectra were collected using Varian Cary 50 spectrophotometer. Steady state fluorescence emission spectra were collected using PTI QuantaMaster 8000 fluorimeter. In all of the cases of the emission collection, slit widths were set to 2 nm on the excitation, and 4 nm on the emission sides.

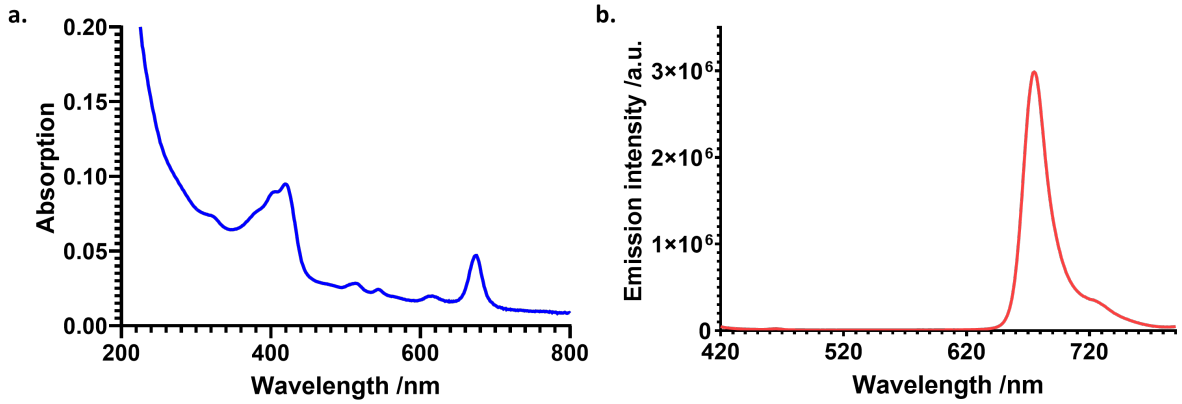

Figure S2: (a.) UV-Visible absorption and (b.) fluorescence emission spectra of the EMPTY PoP liposomes in water. Emission scan was performed with the excitation wavelength set to 410 nm.

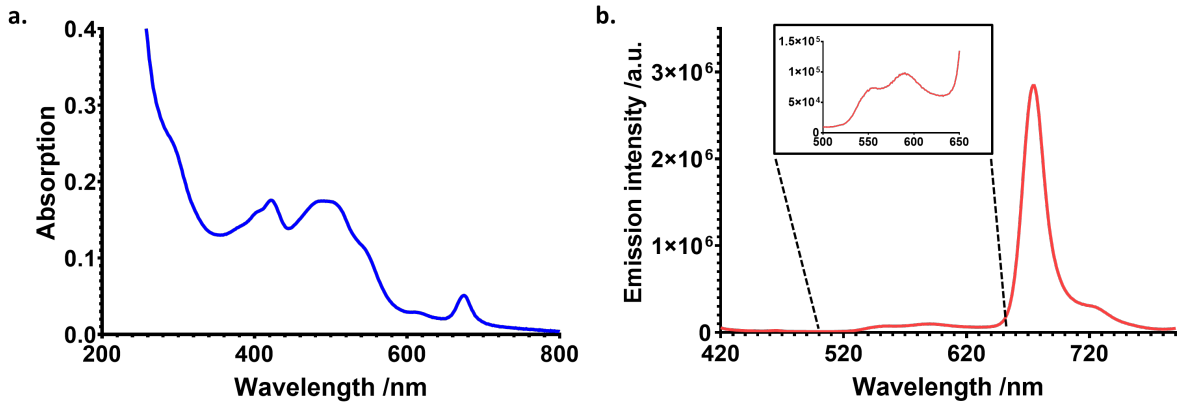

Figure S3: (a.) UV-Visible absorption and (b.) fluorescence emission spectra of the DOX@PoP liposomes in water. Emission scan was performed with the excitation wavelength set to 410 nm. Inset shows a zoomed in area of the overall emission spectrum corresponding to the emission from the doxorubicin, specifically.

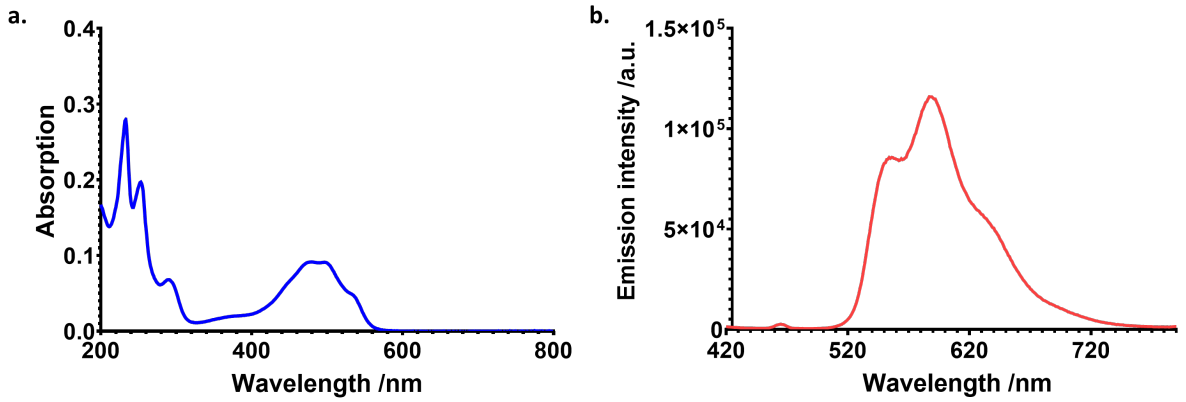

Figure S4: (a.) UV-Visible absorption and (b.) fluorescence emission spectra of doxorubicin sample in water. Emission scan was performed with the excitation wavelength set to 410 nm.

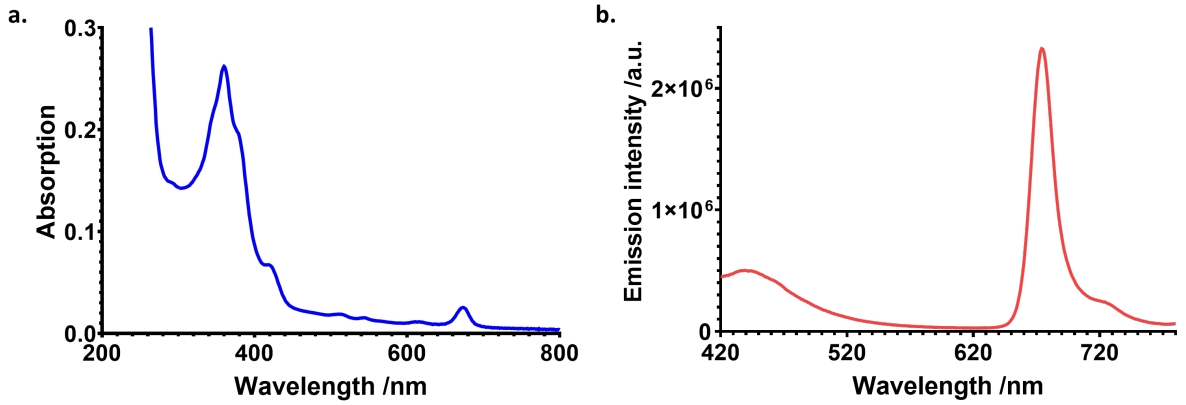

Figure S5: (a.) UV-Visible absorption and (b.) fluorescence emission spectra of the IRT@PoP liposomes in water. Emission scan was performed with the excitation wavelength set to 410 nm.

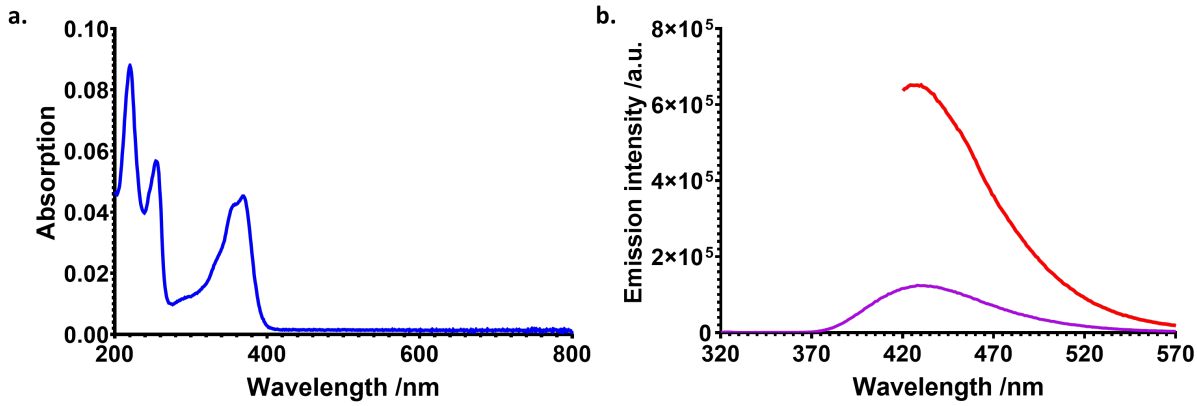

Figure S6: (a.) UV-Visible absorption and (b.) fluorescence emission spectra of irinotecan sample in water. Emission scan was performed with the excitation wavelength set to 410 nm (red) and to 300 nm (purple).

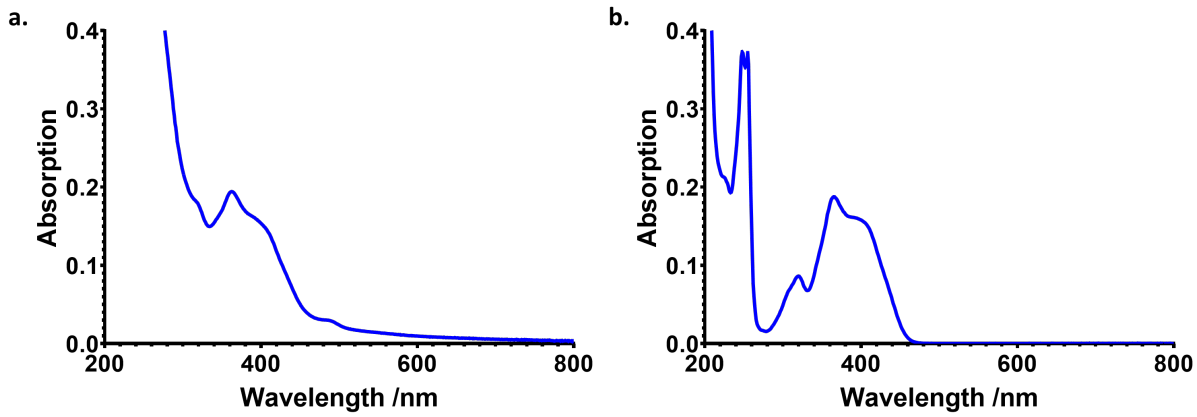

Figure S7: UV-Visible absorption spectra of perinaphthenone (PNN). (a.) PNN@EGG liposomes in H_2O, and (b.) a sample of PNN in H_2O.

3.2 UV-Visible spectra deconvolution

Absorption spectra deconvolution for all liposomes' samples was performed by first subtracting the scattering component from the UV-Visible spectra. Due to the ease of handling, ~120 nm diameter silica nanoparticles (pure light scattering material)[4] were used to obtain a library of scattering profiles at different colloidal concentrations. These profiles were then matched to a specific liposome samples (based on optical density) and subtracted from the original liposomes' UV-Vis spectra to obtain pure absorption spectra. In the case of drug-carrying liposomes, further deconvolution to obtain cargo absorption intensities was performed by fitting and subtracting the pure-absorption spectrum obtained from EMPTY PoP samples from the de-scattered spectra. Results of the deconvolution are presented in figures S8 – S11. Additionally, %contributions to the overall absorption at 355 nm wavelength (used for excitation of samples in direct detection of singlet oxygen phosphorescence – section 4.1 and 4.2) for the porphyrin vs. the encapsulated drugs are reported in table S1.

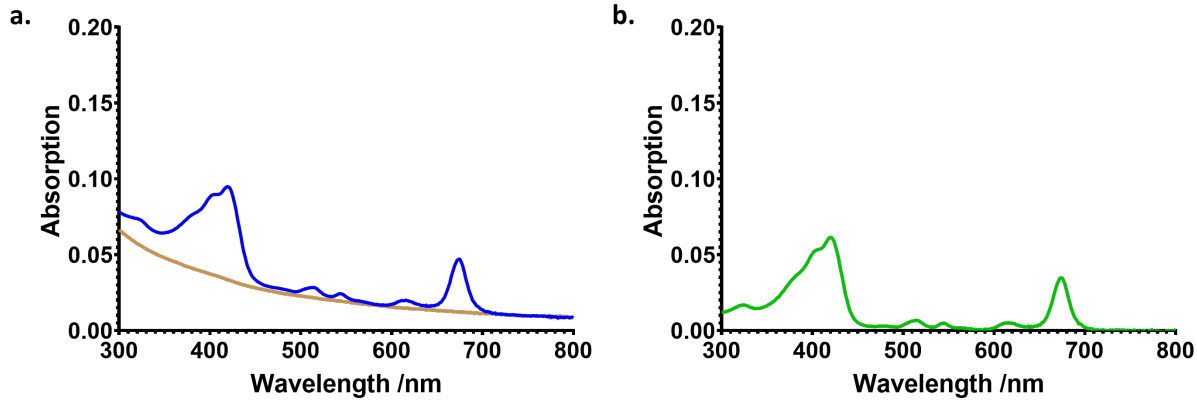

Figure S8: (a.) UV-Visible spectrum of EMPTY PoP liposomes in water (blue) and its matched scattering profile (beige). (b.) The de-scattered, pure-absorption spectrum of EMPTY PoP liposomes in water (green).

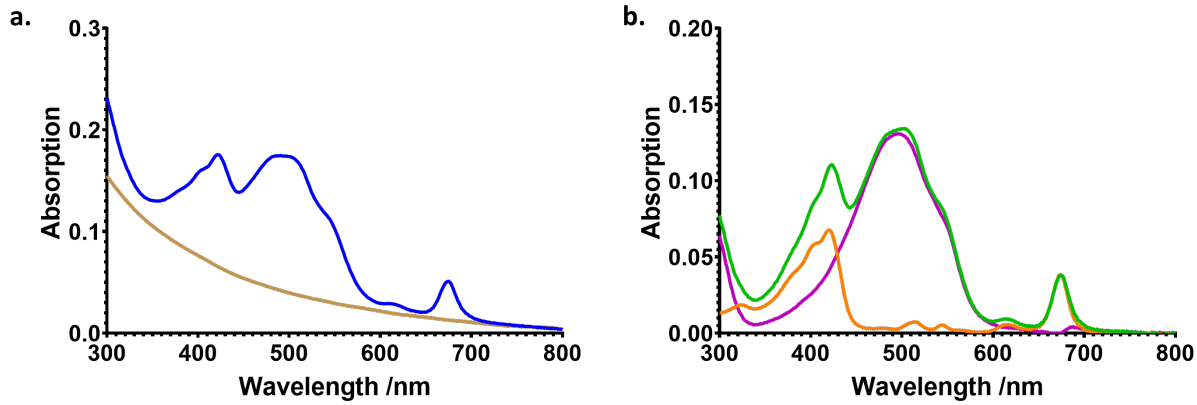

Figure S9: (a.) UV-Visible spectrum of DOX@PoP liposomes in water (blue) and its matched scattering profile (beige). (b.) The de-scattered, pure-absorption spectra of DOX@PoP liposomes in water (green), further separated into the absorption due to the porphyrin dye (orange) and due to the doxorubicin drug (purple).

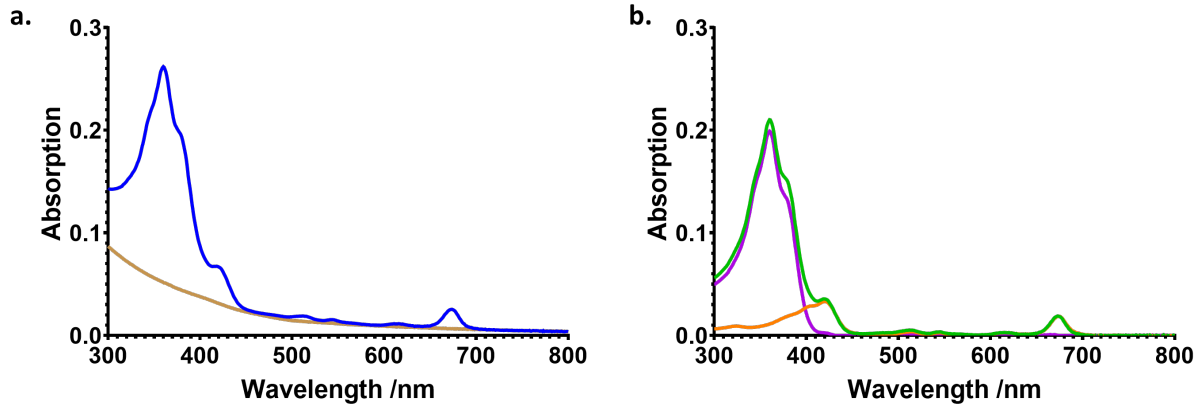

Figure S10: (a.) UV-Visible spectrum of IRT@PoP liposomes in water (blue) and its matched scattering profile (beige). (b.) The de-scattered, pure-absorption spectra of IRT@PoP liposomes in water (green), further separated into the absorption due to the porphyrin dye (orange) and due to the irinotecan drug (purple).

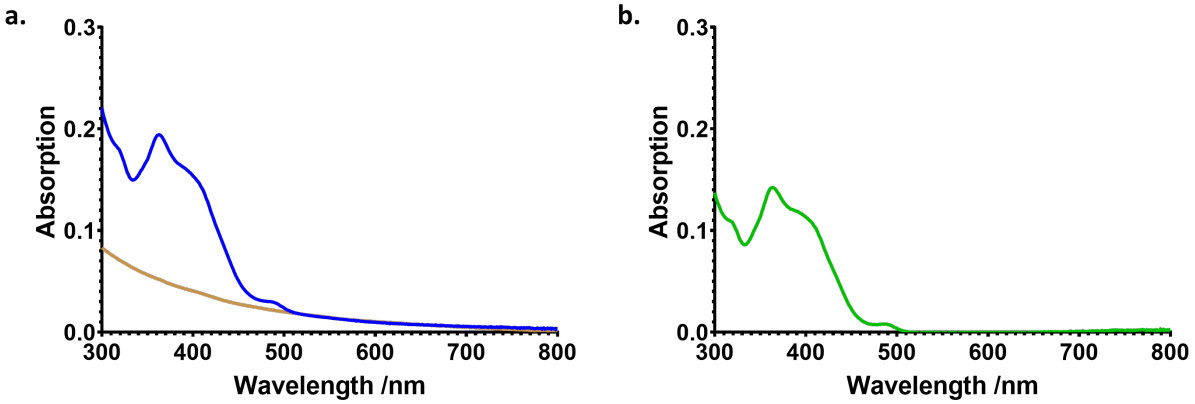

Figure S11: (a.) UV-Visible spectrum of PNN@EGG liposomes in water (blue) and its matched scattering profile (beige). (b.) The de-scattered, pure-absorption spectrum of PNN@EGG liposomes in water (green).

Table S1: Contribution of the porphyrin's and the encapsulated drug's absorption to the total (scattering removed) absorption of PoP liposomes at 355 nm wavelength.

	A_{total} ‡ /absolute (/%contribution)	$A_{porphyrin}$ † /absolute (/%contribution)	A_{cargo} † /absolute (/%contribution)
Empty PoP Liposomes	0.030 (100 %)	0.03 (100%)	-
DOX@PoP Liposomes	0.027 (100%)	0.020 (74%)	0.007 (26%)
IRT@PoP Liposomes	0.193 (100%)	0.010 (5%)	0.183 (95%)

‡ Values based on scattering deconvoluted absorption profiles; † Values based on the fully deconvoluted absorption profiles.

3.3 DOX@PoP drug release ability

Dilute solutions of DOX@PoP liposomes at a concentration of ~0.5 mg/mL were prepared in H_2O and in 95% D_2O. Samples were subjected to irradiation by a CW halogen lamp (300 W, 80 V) on a slide projector (Kodak) mounted with a 625 nm high-pass filter (Figure S12). Thorlabs digital optical energy and power meter console PM100D, equipped with S121C photodiode power sensor was used to measure total light power received by the sample. Samples were set up to receive 110 ± 2 mW of light.

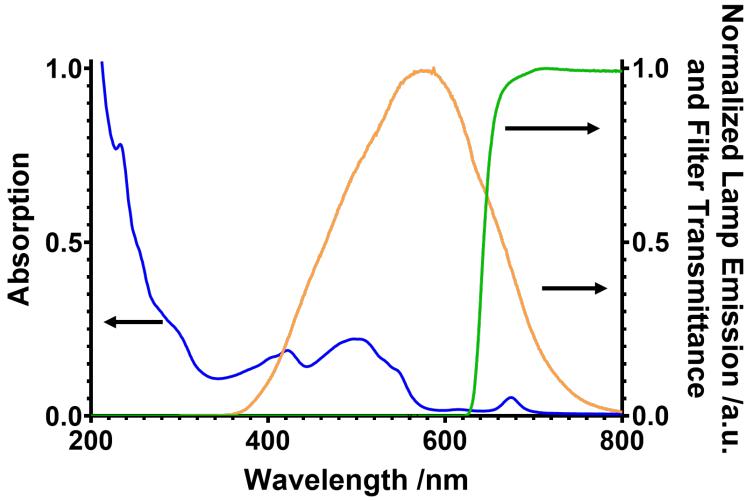

Figure S12: Spectral profile of the Kodak projector lamp used for sample's irradiation (orange), and the UV-Vis transmittance of the 625 nm long-pass filter (green). Additionally shown is the absorption spectrum of DOX@PoP liposomes sample (blue).

Florescence emission of DOX@PoP was used to monitor drug release.[5] After the samples were irradiated for some time interval, an emission measurement was performed using PTI QuantaMaster 8000 fluorimeter. Slit widths were set to 2 nm on the excitation, and 4 nm on the emission sides. The samples were excited at 510 nm wavelength. Results of the drug release experiments are shown in figures S13 and S14. Additionally, DOX@PoP liposomes before and after drug release were characterized for morphology and surface charge changes using dynamic light scattering and Zeta potential measurements (instrumentation details can be found in section 2.2), these results are presented in figure S16.

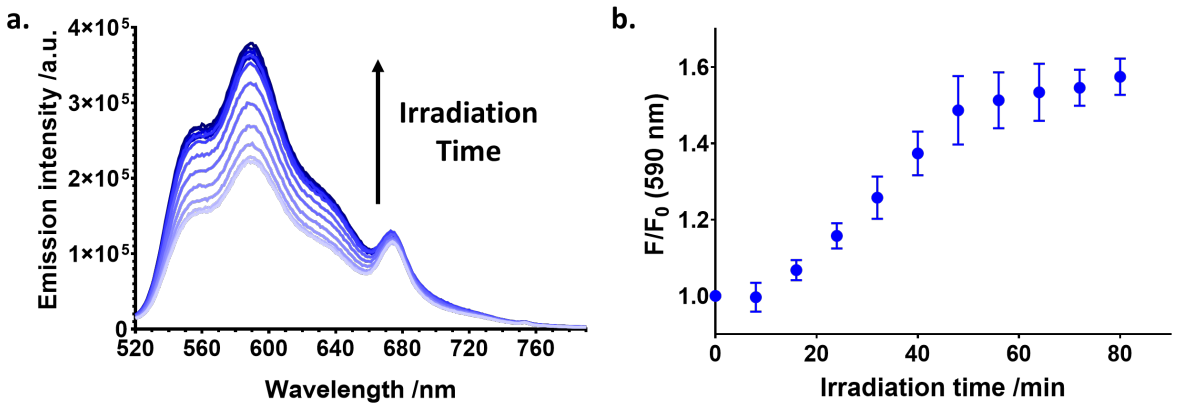

Figure S13: (a.) Steady-state fluorescence emission measurements performed to characterize the release of doxorubicin from DOX@PoP liposomes in H_2O. (b.) Evolution of the doxorubicin's peak fluorescence emission at 590 nm as a result of selective irradiation of the porphyrin in DOX@PoP liposomes. Error bars represent standard deviation between triplicate experiments.

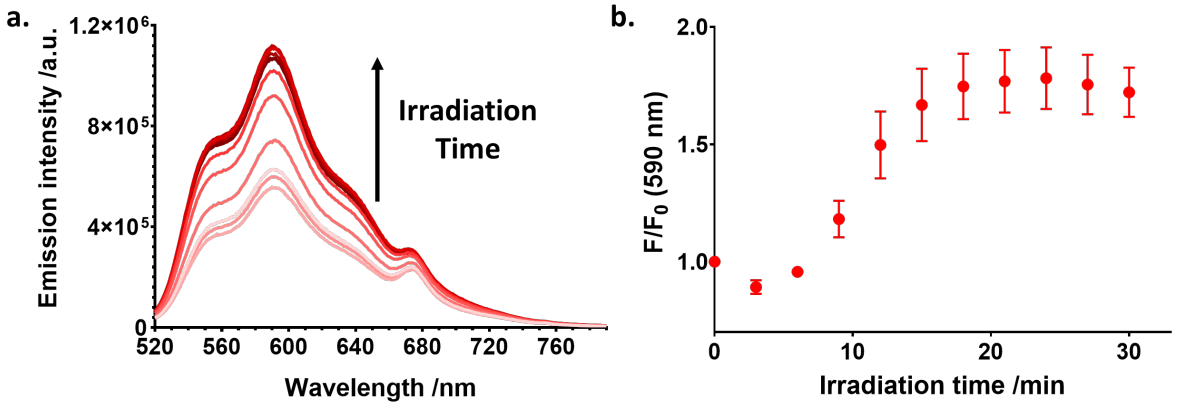

Figure S14: (a.) Steady-state fluorescence emission measurements performed to characterize the release of doxorubicin from DOX@PoP liposomes in 95% D_2O. (b.) Evolution of the doxorubicin's peak fluorescence emission at 590 nm as a result of selective irradiation of the porphyrin in DOX@PoP liposomes. Error bars represent standard deviation between triplicate experiments.

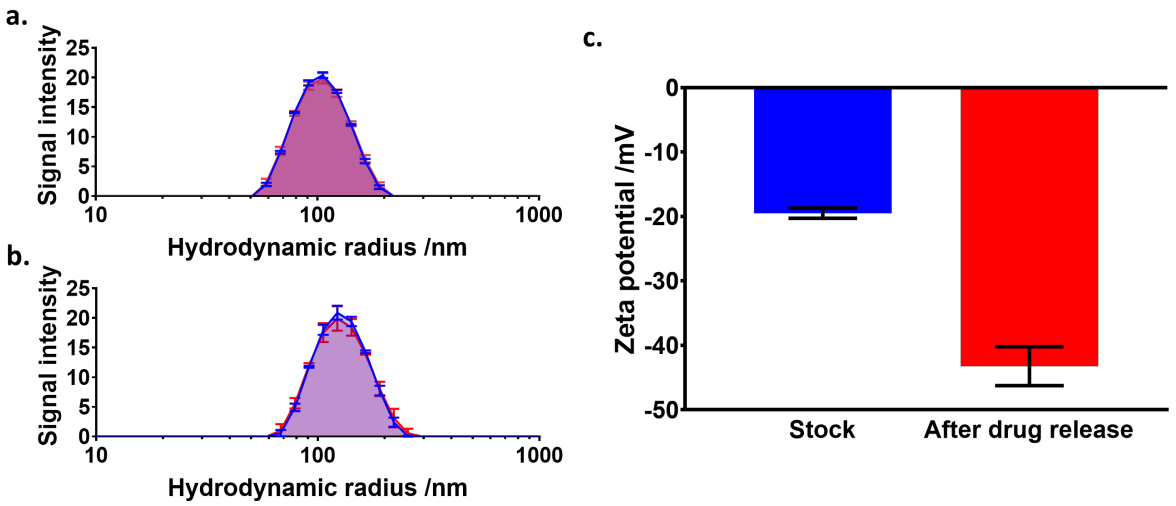

Figure S15: Size distribution of DOX@PoP liposomes sample in water before (blue) and after (red) light induced drug release in H_2O (a.) and in 95% D_2O (b.). (c.) Surface charge as characterized by the Zeta potential for DOX@PoP liposomes before and after drug release. Error bars represent standard deviation between triplicate measurements.

4. Singlet oxygen detection

4.1 Time-resolved direct detection of singlet oxygen phosphorescence

Time resolved near-infrared (NIR) phosphorescence of $^1O_2$ was detected using a customized system.[6] A diode-pumped pulsed Nd:YAG laser (FTSS355-Q, Crystal Laser, Berlin, Germany) working at 1 kHz repetition rate at 355 nm or 532 nm was used for excitation. A 1064 nm rugate notch filter (Edmund Optics, York, U.K.) was placed at the exit port of the laser to remove any residual component of its fundamental emission in the near-infrared region. The $^1O_2$ luminescence exiting from the sample was detected at 90° angle via a Hamamatsu NIR detector (cooled to -62.8°C operating at 800 V) coupled to a grating monochromator (Spectral Products, CM110). Photon counting was achieved with a multichannel scaling card (NanoHarp 250, PicoQuant Gmbh, Germany).

The production of $^1O_2$ via photosensitization can be viewed as a two-step process in which light energy is first absorbed by a photosensitizer (PS) and then transferred to molecular oxygen to produce $^1O_2$ (Scheme S1). Absorption of light by the PS promotes it to its excited singlet state $^1PS^*$. This state can further evolve over time (intersystem crossing, k_{ISC}) to the lower-lying triplet excited state, $^3PS^*$, in competition with radiative (fluorescence, k_F) and non-radiative (internal conversion, k_{IC}) decay back to the ground state. $^3PS^*$ may then transfer its energy to molecular oxygen, $^3O_2$, to produce $^1O_2$ (fast) or decay back to the ground state (slow, k_T). Therefore, it is adequate to state that the rate of $^1O_2$ production is equal to the rate of ^3PS decay, and the time constant of the process is therefore the triplet lifetime τ_T *(= 1/k_T)*. Once produced, $^1O_2$ will disappear with a lifetime, τ_Δ, mostly through non-radiative processes ($k_{\Delta, nr}$),[7] but a minor fraction of $^1O_2$ molecules will emit a photon in the near-infrared spectral region ($k_{\Delta, r}$).[8]

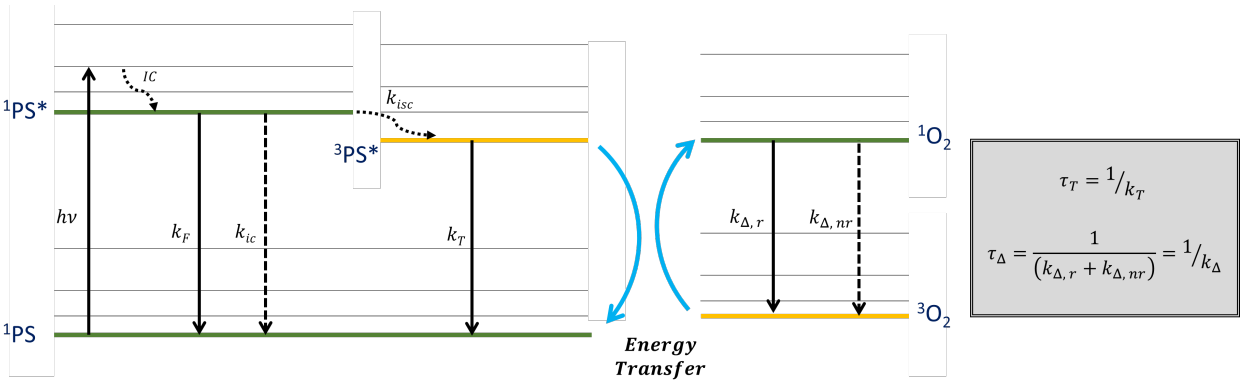

Scheme S1: Production of $^1O_2$ by a photosensitizer (PS), where hν represents an absorbed photon, k_{IC} is the internal conversion rate constant, k_{ISC} is the intersystem crossing rate constant, k_F is the fluorescence rate constant, k_T is the triplet PS rate constant, $k_{\Delta,r}$ is the radiative rate constant for $^1O_2$ deactivation, $k_{\Delta,nr}$ is the non-radiative rate constant for $^1O_2$ deactivation, τ_T is the triplet lifetime and τ_Δ is the $^1O_2$ lifetime.

According to scheme S1, the basic kinetic parameters that contribute to the $^1O_2$ production and decay are the ^{3}PS lifetime, τ_T, and the $^1O_2$ lifetime, τ_Δ. Therefore, the phosphorescence signal (S_t) of $^1O_2$ detected at 1270 nm presents a rise and decay bi-exponential behaviour, which can be modelled by the expression given by equation S1. S_0 is the measure of the signal strength, directly linked to the amount of singlet oxygen in solution, while the term Y_0 is added to account for the baseline in the real measurement.[9]

$$S_t = S_0 \times \frac{\tau_\Delta}{\tau_\Delta - \tau_T} \times \left(e^{-t/\tau_\Delta} - e^{-t/\tau_T}\right) + Y_0 \qquad (Eq.S1)$$

Singlet oxygen phosphorescence decay signals were collected at 1270 nm. Unless stated otherwise, all samples were irradiated at 355 nm excitation wavelength, and the decay curves for the samples in H_2O were collected in 600 seconds, while for samples in 95% D_2O in 300 seconds. The signals were collected with 256 ns resolution. The kinetic traces were least-squares fitted to equation S1 typically in 1200 ns to 300000 ns time window using Prism 8.0 software (GraphPad Software Inc., La Jolla, CA) with τ_Δ, τ_T, S_0 and Y_0 as free parameters. The quality of the fittings was assessed by the residual plots. For the PoP liposomes' samples, the experimental results and fit parameters are summarized in figures S16 – S19, and table S2. For the reference compounds, the experimental results and fit parameters are summarized in figures S20 – S23, and table S3. Singlet oxygen lifetimes in solutions containing irinotecan and doxorubicin at various concentrations are presented in figures S24 and S25.

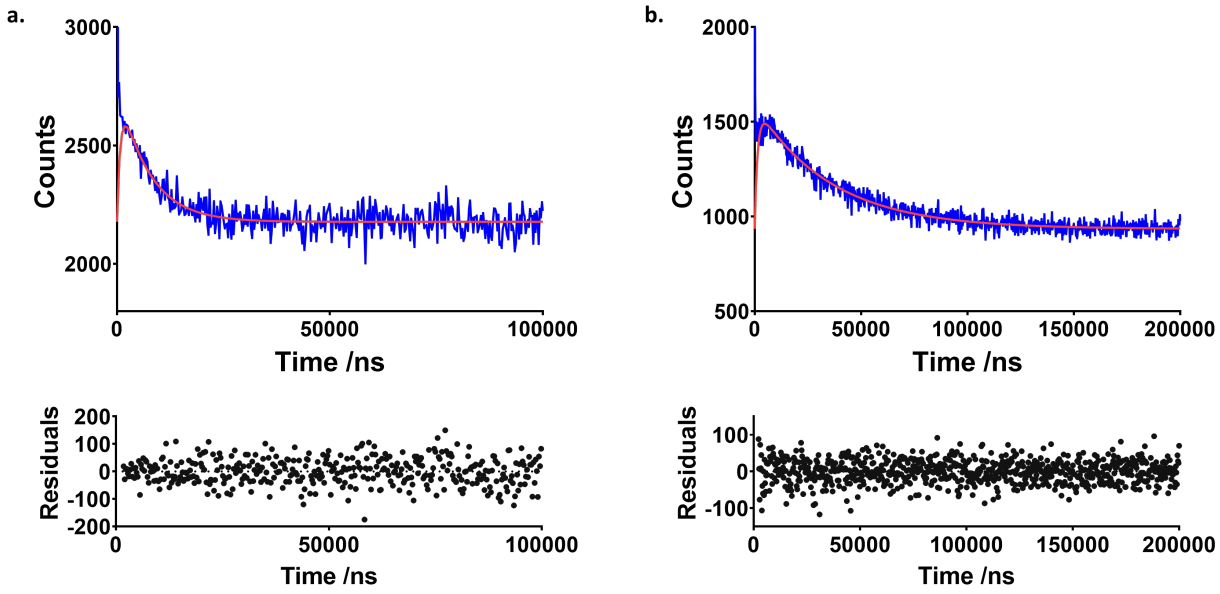

Figure S16: Time-resolved $^1O_2$ phosphorescence signals at 1270 nm (blue) and the corresponding fittings (red) obtained on the sample of EMPTY PoP liposomes in H_2O (a.), and in 95% D_2O (b.) Residuals obtained from the fits are shown in black below each respective plot.

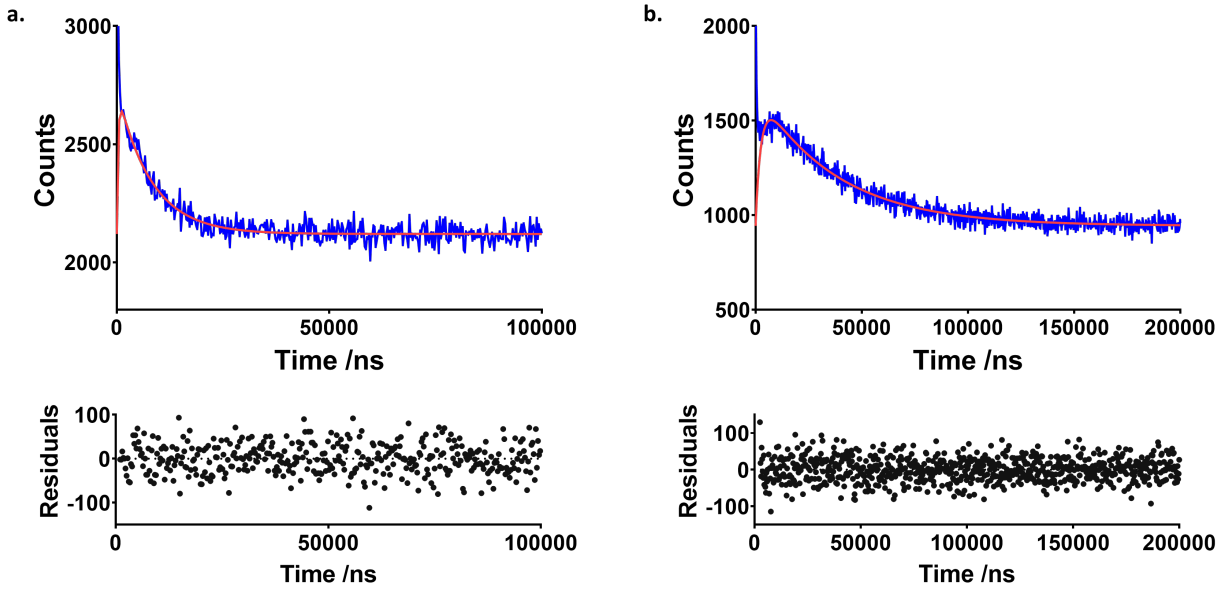

Figure S17: Time-resolved $^1O_2$ phosphorescence signals at 1270 nm (blue) and the corresponding fittings (red) obtained on the sample of DOX@PoP liposomes in H_2O (a.), and in 95% D_2O (b.). Residuals obtained from the fits are shown in black below each respective plot.

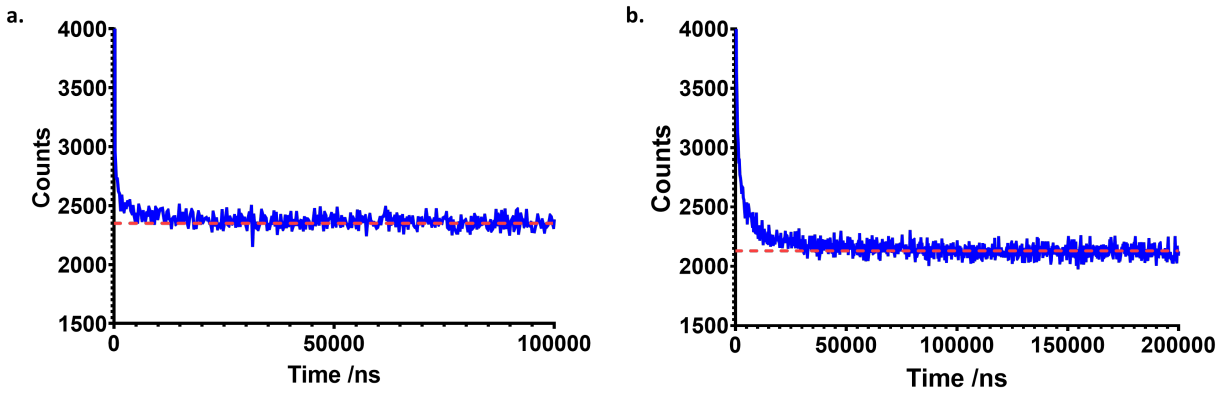

Figure S18: Time-resolved $^1O_2$ phosphorescence signals at 1270 nm (blue) obtained on the sample of nitrogen purged DOX@PoP liposomes in H_2O (a.), and in 95% D_2O (b.). Signal collection time was set to 600 seconds in both H_2O and 95% D_2O. Flat red dotted lines are shown for clarity.

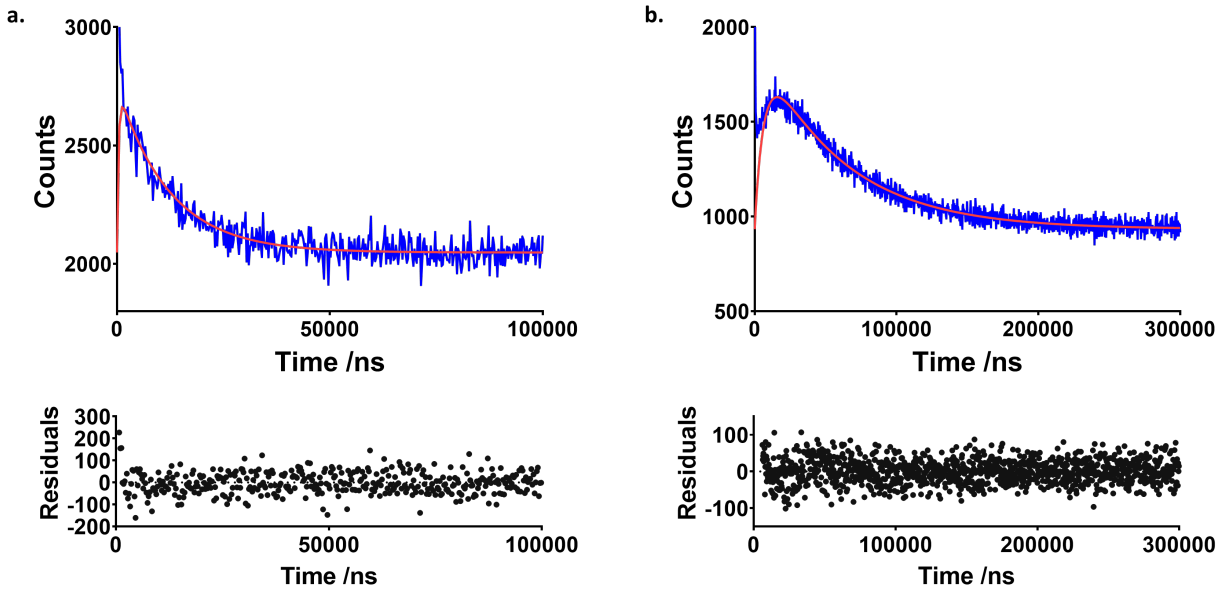

Figure S19 Time-resolved $^1O_2$ phosphorescence signals at 1270 nm (blue) and the corresponding fittings (red) obtained on the sample of IRT@PoP liposomes in H_2O (a.), and in 95% D_2O (b.) Residuals obtained from the fits are shown in black below each respective plot.

Table S2: Singlet oxygen phosphorescence decay curve fits' parameters for a range of PoP Liposome samples.[†]

	Empty PoP (H_2O)	Empty PoP (95% D_2O)	DOX@PoP (H_2O)	DOX@PoP (95% D_2O)	IRT@PoP (H_2O)	IRT@PoP (95% D_2O)
S_0/counts	535 ± 27	634 ± 6	594 ± 14	681 ± 7	713 ± 16	915 ± 7
τ_Δ/μs	7.1 ± 0.6	35.6 ± 0.7	8.0 ± 0.3	37.3 ± 0.8	11.1 ± 0.4	58.4 ± 0.9
$\tau_{triplet}$/μs	0.8 ± 0.3	1.4 ± 0.1	0.3 ± 0.1	2.5 ± 0.1	~0.3	6.4 ± 0.2
Y_0/counts	2178 ± 3	935 ± 2	2121 ± 2	944 ± 2	2051 ± 3	934 ± 2

[†] Errors are based on the standard deviation of fitting equation S3 to the experimental data

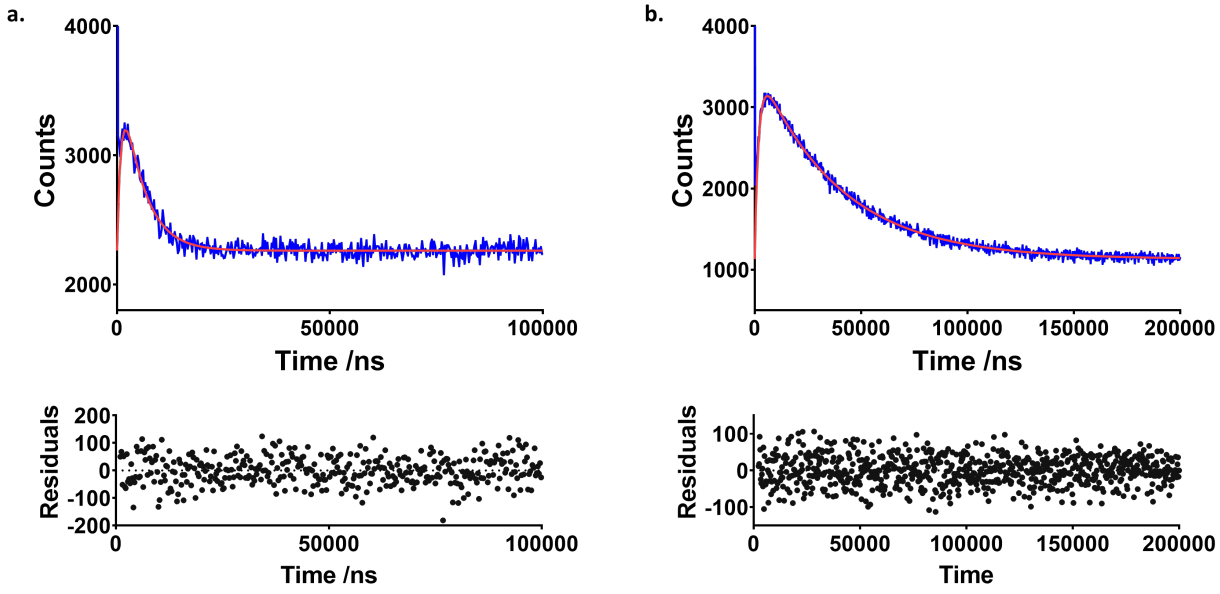

Figure S20: Time-resolved $^1O_2$ phosphorescence signals at 1270 nm (blue) and the corresponding fittings (red) obtained on the sample of PNN@EGG liposomes in H_2O (a.), and in 95% D_2O (b.). Residuals obtained from the fits are shown in black below each respective plot.

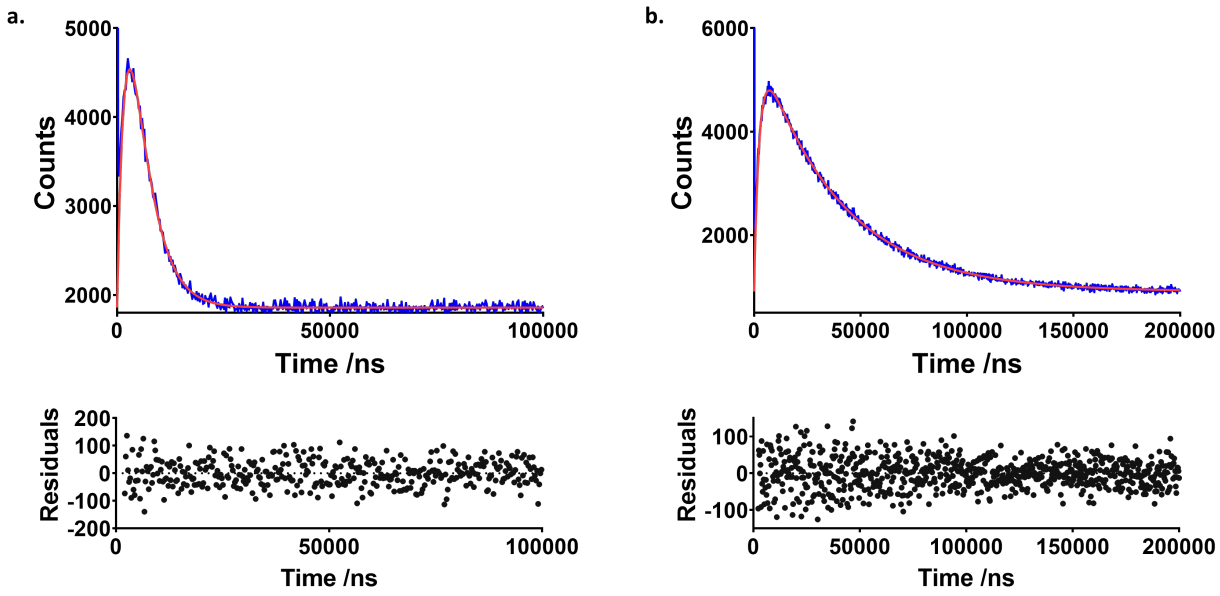

Figure S21: Time-resolved $^1O_2$ phosphorescence signals at 1270 nm (blue) and the corresponding fittings (red) obtained on the sample of riboflavin photosensitizer in H_2O (a.), and in 95% D_2O (b.). Residuals obtained from the fits are shown in black below each respective plot.

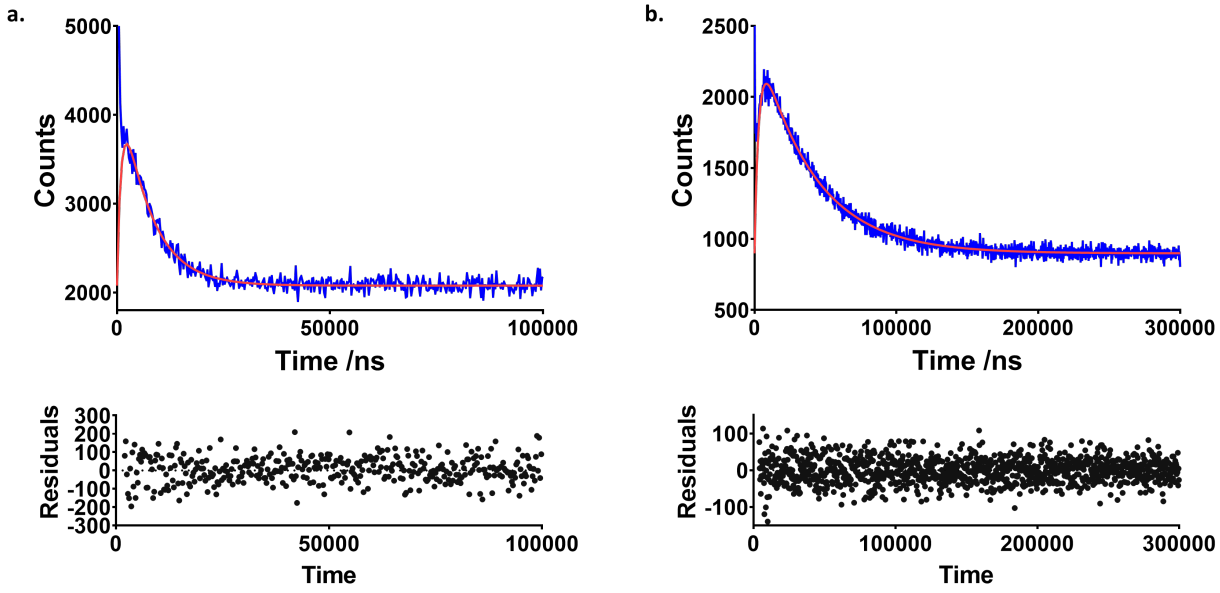

Figure S22: Time-resolved $^1O_2$ phosphorescence signals at 1270 nm (blue) and the corresponding fittings (red) obtained on the sample of irinotecan free in solution of H_2O (a.), and in 95% D_2O (b.). Residuals obtained from the fits are shown in black below each respective plot.

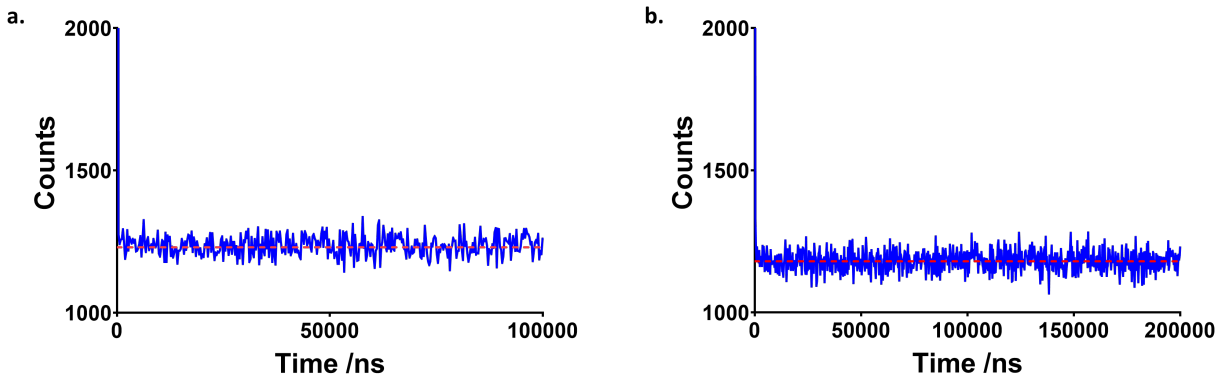

Figure S23: Time-resolved $^1O_2$ phosphorescence signals at 1270 nm (blue) obtained on the sample of doxorubicin free in solution of H_2O (a.), and in 95% D_2O (b.). Signal collection time was set to 300 seconds in both H_2O and 95% D_2O. Flat red dotted lines are shown for clarity.

Table S3: Singlet oxygen phosphorescence decay curve fit parameters for reference samples. [†]

	PNN@EGG (H_2O)	**PNN@EGG (95% D_2O)**	**Riboflavin (H_2O)**	**Riboflavin (95% D_2O)**	**IRT (H_2O)**	**IRT (95% D_2O)**	**DOX**
S_0/*counts*	1412 ± 47	2351 ± 8	5398 ± 144	4692 ± 9	2219 ± 44	1481 ± 7	N.D.
τ_Δ/*μs*	4.9 ± 0.2	38.2 ± 0.3	4.2 ± 0.1	37.9 ± 0.2	6.8 ± 0.2	39.0 ± 0.3	
$\tau_{triplet}$/*μs*	1.01 ± 0.09	1.90 ± 0.04	2.16 ± 0.09	2.44 ± 0.02	1.0 ± 0.1	3.03 ± 0.08	
Y_0/*counts*	2261 ± 3	1130 ± 3	1858 ± 3	911 ± 3	2078 ± 3	899 ± 1	

[†] Errors are based on the standard deviation of fitting equation S3 to the experimental data

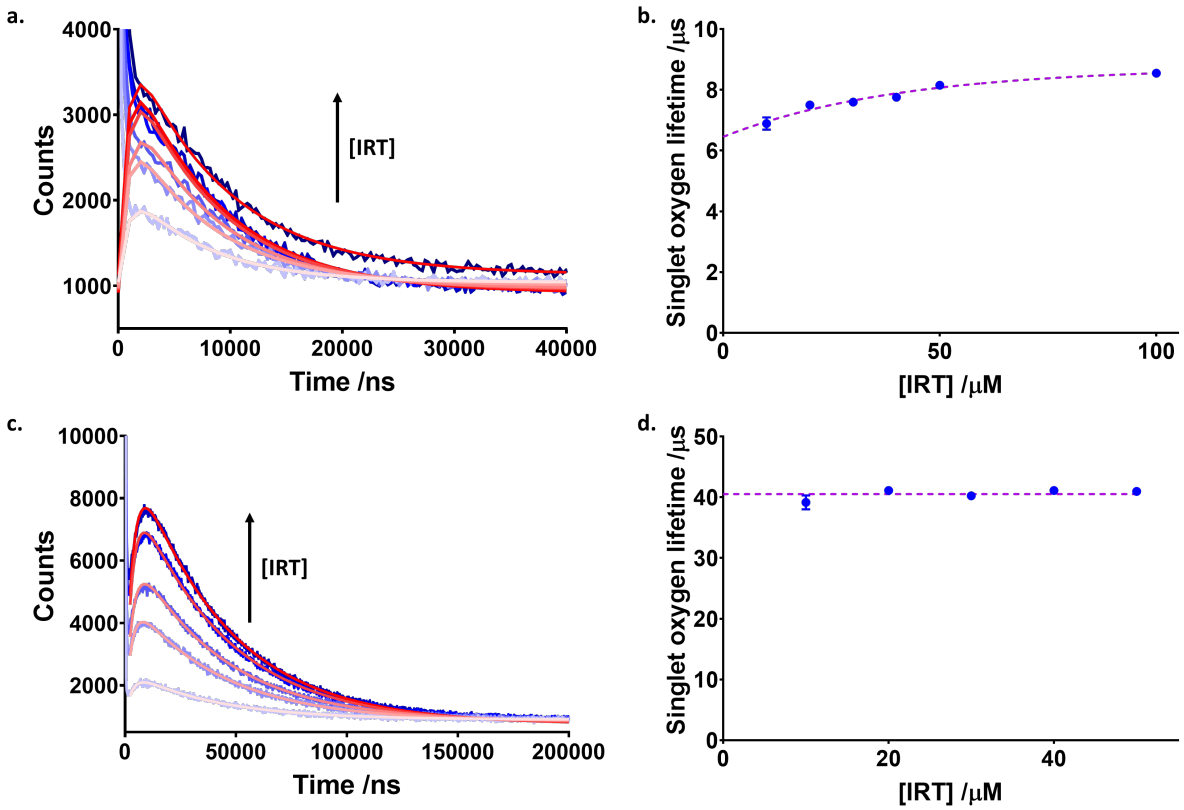

Figure S24: Time-resolved $^1O_2$ phosphorescence signals at 1270 nm (blue) and the corresponding fits (red) obtained on the samples of irinotecan at different concentrations in H_2O (a.), and in 95% D_2O (c.). Signal collection time was set to 300 seconds in both H_2O and 95% D_2O. Singlet oxygen lifetimes detected from samples of various concentrations of irinotecan in H_2O (b. $\tau_{plateau\text{-}H2O}$ = 8.7 ± 0.3 µs) and 95% D_2O (d. τ_{D2O} = 40.5 ± 0.3 µs). Error bars represent standard deviation obtained from the fits.

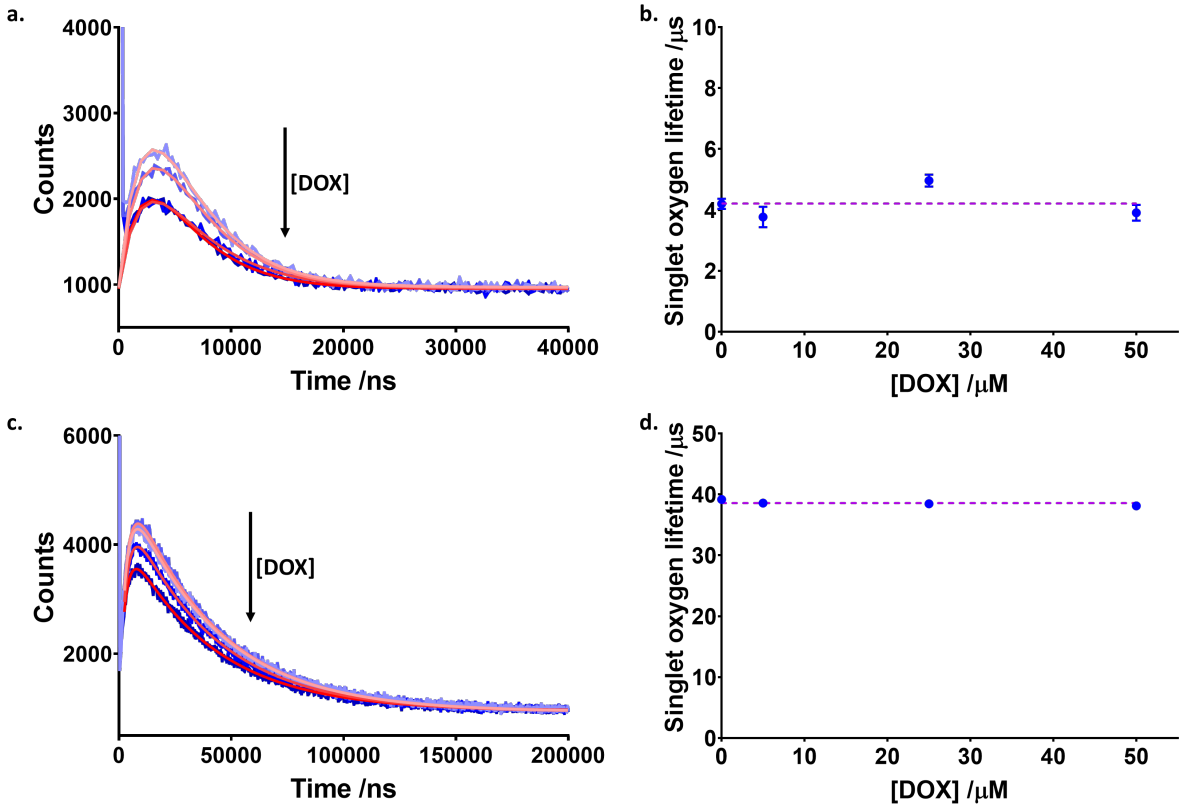

Figure S25: Time-resolved $^1O_2$ phosphorescence signals at 1270 nm (blue) and the corresponding fits (red) obtained on the samples of riboflavin in the presence of different concentrations of doxorubicin in H_2O (a.), and in 95% D_2O (c.). Signal collection time was set to 300 seconds in both H_2O and 95% D_2O. Singlet oxygen lifetimes detected from samples of riboflavin mixed with various concentrations of doxorubicin in H_2O (b. τ_{H2O} = 4.2 ± 0.3 µs) and 95% D_2O (d. τ_{D2O} = 38.6 ± 0.2 µs). Error bars represent standard deviation obtained from the fits.

4.2 Indirect detection of singlet oxygen production

Irradiation of samples was performed using a CW halogen lamp (300 W, 80 V) on a slide projector (Kodak) mounted with a 295 nm cut-off high-pass filter (Figure S27). Thorlabs digital optical energy and power meter console PM100D, equipped with S121C photodiode power sensor was used to measure light power received by the sample. Samples were set up to receive a total of 8.00 ± 0.02mW of light. As can be seen in figure S26, the experimental set up ensured selective irradiation of the photosensitizer systems (IRT@PoP liposomes shown as sample) without the irradiation of the singlet oxygen sensitive molecular probe, uric acid ($\lambda_{abs.max}$ = 291 nm). Irradiation experiments were performed in H_2O buffered with sodium phosphate buffer to pH = 7.4. Control experiments to ensure selectivity of uric acid towards singlet oxygen were performed by also carrying out the irradiation experiments on N_2 purged samples.

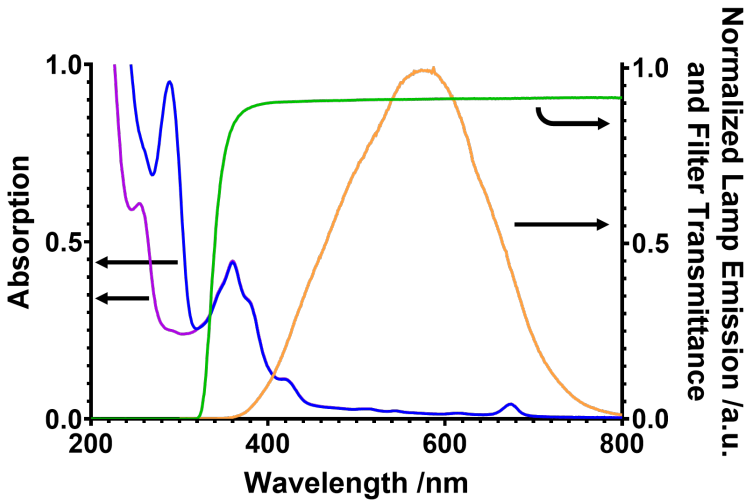

Figure S26: Spectral profile of the Kodak projector lamp used for sample's irradiation (orange), and the UV-Vis transmittance of the 295 nm long-pass filter (green). Additionally shown, are the absorption profiles of IRT@PoP liposome samples with uric acid (blue) and without uric acid (purple).

Consider the following general photochemical processes, and their assigned rate constants, occurring in a solution containing a photosensitizer and a $^1O_2$ sensor, in our case uric acid (UA):

Light absorption	$^1PS + h\nu \rightarrow {}^1PS^*$	
Intersystem crossing	$^1PS^* \rightarrow {}^3PS^*$	k_{ISC}
Energy transfer	$^3O_2 + {}^3PS^* \rightarrow {}^1O_2 + {}^1PS$	k_{ET}
Singlet oxygen deactivation by the environment	$^1O_2 \rightarrow {}^3O_2$	k_Δ
Physical quenching by sensor	$^1O_2 + UA \rightarrow {}^3O_2 + UA$	k_p
Chemical interaction with sensor	$^1O_2 + UA \rightarrow$ degradation products	k_{ox}

Importantly, for the photosensitizers free in solution the singlet oxygen deactivation by the environment is dominated by the solvent. However, in the case of liposome entrapped photosensitizers, we can describe singlet oxygen deactivation by the environment (k_Δ) as a combination of its deactivation in the lipid membrane (k_{lipid}), internal liposome cavity (k_{in}), and the external solution environment (k_{out}).

The external liposomal environment		$^1O_2 + H_2O/D_2O \rightarrow {}^3O_2 + H_2O/D_2O$	k_{out}
The lipid membrane	(physical)	$^1O_2$ + lipid→ $^3O_2$ + lipid	$k_{lipid,\ p}$
	(chemical)	$^1O_2$ + lipid→ oxidation products	$k_{lipid,\ ox}$
The internal liposomal environment	(physical)	$^1O_2 + H_2O/D_2O \rightarrow {}^3O_2 + H_2O/D_2O$	$k_{in,\ p}$
	(chemical)	$^1O_2$ + cargo → degradation products	$k_{in,\ ox}$

In all cases, we will assume that the direct reaction of PS in its ground state and $^1O_2$ is negligible. Additionally, in the case of liposome systems we will also simplify by combining physical and chemical deactivation pathways in the lipid membrane ($k_{lipid,\ p} + k_{lipid,\ ox}[lipid] = k_{lipid}$), and in the internal liposomal environment ($k_{in,\ p} + k_{in,\ ox}[cargo] = k_{in}$). Each one of the three environments will have some fractional contribution (g) to the observed, that is the total, rate of deactivation. Therefore, the observed rate of deactivation of $^1O_2$ can be described by equation S2, with the relationship between the values of g given by equation S3.

$$k_\Delta = g^{out}k_{out} + g^{lipid}k_{lipid} + g^{in}k_{in} \qquad (Eq.S2)$$

$$g^{out} + g^{lipid} + g^{in} = 1 \qquad (Eq.S3)$$

Under steady state approximation, i.e. no significant buildup of $^1O_2$ is expected, rate of the sensor disappearance can be written following equation S4, with Φ_Δ representing the quantum yield of photosensitization, and I_{Abs} being the integrated intensity of the absorbed light obtained via equation S5. Importantly, for liposome systems we must also introduce a term g^{out} into the equation, as singlet oxygen is only detected by the chemical sensor in the external liposomal environment. It follows, that for photosensitizers free in solution g^{out} is equal to 1.

$$\frac{d[UA]}{dt} = -g^{out}\,k_{ox}\,[UA][\,^1O_2] = -g^{out}\,k_{ox}\,[UA]\frac{\Phi_\Delta I_{Abs}}{\left(k_{ox} + k_p\right)[UA] + k_\Delta} \qquad (Eq.S4)$$

$$I_{Abs} = \int_{200\,nm}^{800\,nm} I_{source}(\lambda) * T_{filter}(\lambda) * \left(1 - 10^{-A(\lambda)}\right) d\lambda \quad (Eq.S5)$$

In the equation S5, the term $I_{source}(\lambda)$ is the intensity of the light source at wavelength λ, $T_{filter}(\lambda)$ is the transmittance of the filter at wavelength λ, and $A(\lambda)$ is the absorption (deconvoluted from scattering) of the sample at wavelength λ. Percent contributions to the overall integrated absorption in the irradiation range of wavelengths for the porphyrin vs. the encapsulated drugs are reported in table S4.

In our case the concentration of uric acid was 5×10^{-5} M, while the overall rate constant for UA mediated removal of singlet oxygen $(k_{ox}+k_p)$ has been reported to be 3.6×10^8 M^{-1} s^{-1}.[10] This means that the term $(k_{ox}+k_p)[UA]$ is much smaller than the rate of singlet oxygen deactivation by the environment (based on data reported in section 4.1, k_Δ is in the 10^5 order of magnitude), therefore S4 can be simplified to:

$$\frac{d[UA]}{dt} = -g^{out} k_{ox}[UA] \frac{\Phi_\Delta I_{Abs}}{k_\Delta} = -k_{PS}[UA] \quad (Eq.S7)$$

Where, the rate constant k_{PS} is simply a combination of a few constants given by equation S8.

$$k_{PS} = -g^{out} \times k_{ox} \times \Phi_\Delta \times I_{Abs} \times \frac{1}{k_\Delta} \quad (Eq.S8)$$

The overall rate of UA degradation can then be viewed as pseudo first order, or mathematically in the form of equation S9.

$$\ln[UA]_t = \ln[UA]_0 - k_{PS}t \quad (Eq.S9)$$

By monitoring the sensor (UA) degradation, values of k_{PS} are determined experimentally for the various PS systems according to equation S9. Results of the irradiation experiments of a range of PoP Liposomes are presented in figure S27 – S29.

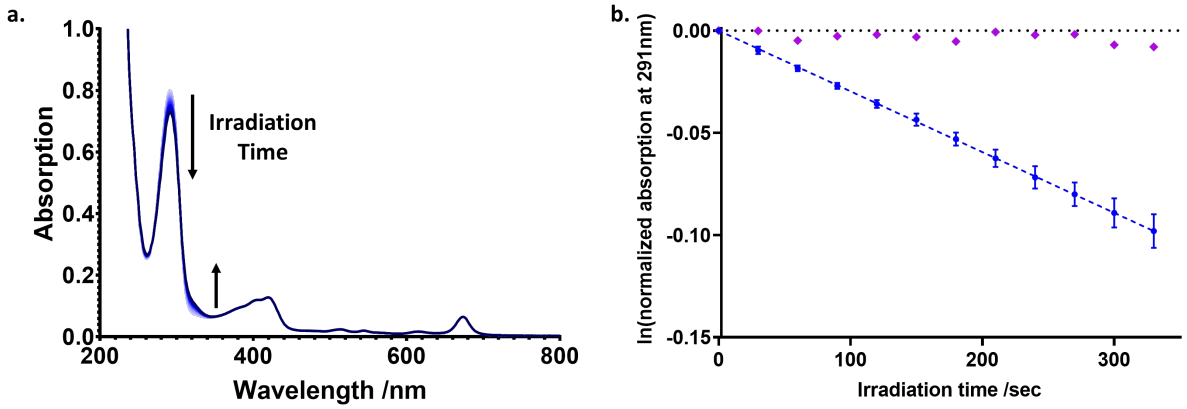

Figure S27: (a.) Singlet oxygen production from EMPTY PoP liposomes in H_2O, as detected via the indirect detection methodology using uric acid (λ_{abs} = 291 nm) as the singlet oxygen sensitive probe. (b.) Evolution of uric acid absorption loss due to the selective irradiation of EMPTY PoP liposomes under air equilibrated (blue spheres) and nitrogen purged (purple diamonds) conditions. Line of best-fit is shown as blue dotted line with a slope of 2.97 ± 0.02 × 10^{-4} s^{-1}. Error bars correspond to the standard error from triplicate measurements.

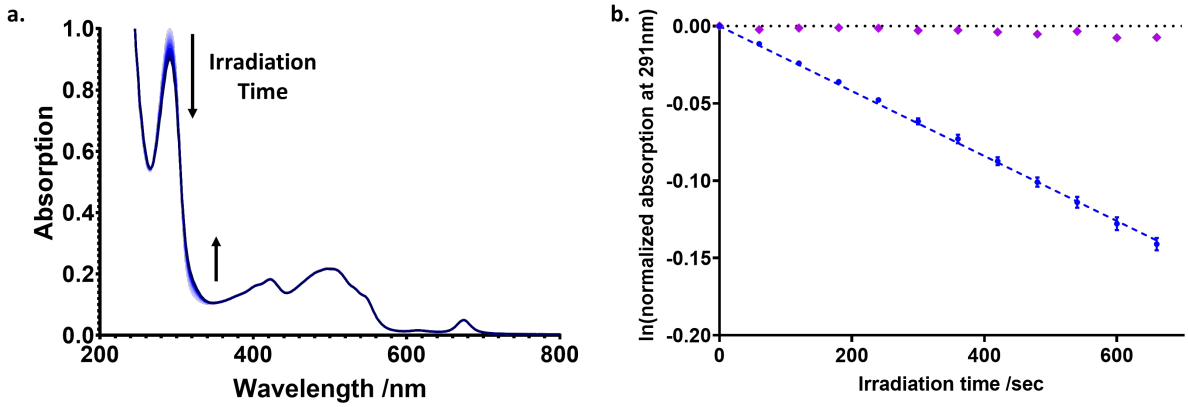

Figure S28: (a.) Singlet oxygen production from DOX@PoP liposomes in H_2O, as detected via the indirect detection methodology using uric acid (λ_{abs} = 291 nm) as the singlet oxygen sensitive probe. (b.) Evolution of uric acid absorption loss due to the selective irradiation of DOX@PoP liposomes under air equilibrated (blue spheres) and nitrogen purged (purple diamonds) conditions. Line of best-fit is shown as blue dotted line with a slope of 2.10 ± 0.03 × 10^{-4} s^{-1}. Error bars correspond to the standard error from triplicate measurements.

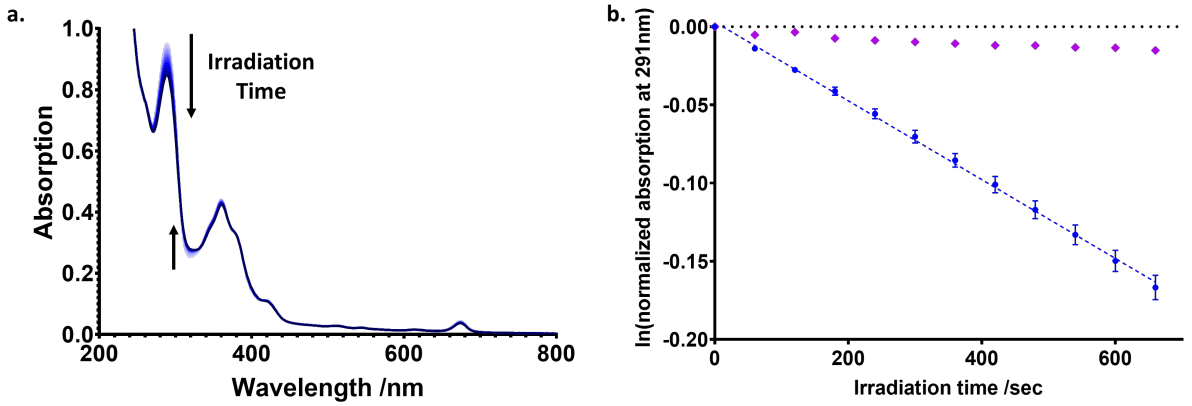

Figure S29: (a.) Singlet oxygen production from IRT@PoP liposomes in H_2O, as detected via the indirect detection methodology using uric acid (λ_{abs} = 291 nm) as the singlet oxygen sensitive probe. (b.) Evolution of uric acid absorption loss due to the selective irradiation of IRT@PoP liposomes under air equilibrated (blue spheres) and nitrogen purged (purple diamonds) conditions. Line of best-fit is shown as blue dotted line with a slope of 2.52 ± 0.03 × 10^{-4} s^{-1}. Error bars correspond to the standard error from triplicate measurements.

Table S4: Contribution of the porphyrin's and the encapsulated drug's absorption to the integrated total (scattering removed) absorption of PoP liposomes in the indirect singlet oxygen detection set up.

	I_{Abs}^{total} ‡ /absolute (/%contribution)	$I_{Abs}^{porphyrin}$ † /absolute (/%contribution)	I_{Abs}^{cargo} † /absolute (/%contribution)
Empty PoP Liposomes	4.44 (100 %)	4.44 (100 %)	-
DOX@PoP Liposomes	27.01 (100%)	3.35 (12%)	23.66 (88%)
IRT@PoP Liposomes	3.54 (100%)	2.58 (73%)	0.96 (27%)

‡ Values based on scattering deconvoluted absorption profiles; † Values based on the fully deconvoluted absorption profiles.

4.3 Indirect (apparent) singlet oxygen production quantum yields

In order to calculate $\Phi_{\Delta}^{apperent}$ for a range of PoP liposomes, equation S8 can be rewritten in terms of the apparent singlet oxygen lifetime in solution, as characterized via the direct detection (section 4.1), for the reference photosensitizer system (R) and for the liposomes samples (S), given by equations S10 and S11, respectively. As was previously mentioned, singlet oxygen produced from the reference photosensitizer in homogeneous environment spends all of its lifetime in the solvent, thus by definition, value of g^{out} for the reference is equal to 1.

$$k_{PS}^{R} = -g^{out} \times k_{ox} \times \Phi_{\Delta}^{R} \times I_{Abs}^{R} \times \tau_{\Delta}^{R} = -1 \times k_{ox} \times \Phi_{\Delta}^{R} \times I_{Abs}^{R} \times \tau_{\Delta}^{R} \qquad (Eq.S10)$$

$$k_{PS}^{S} = -g^{out} \times k_{ox} \times \Phi_{\Delta}^{S} \times I_{Abs}^{S} \times \tau_{\Delta}^{S} = -k_{ox} \times \Phi_{\Delta}^{apparent} \times I_{Abs}^{S} \times \tau_{\Delta}^{S} \qquad (Eq.S11)$$

Where, $\Phi_{\Delta}^{apperent}$ is defined by equation S12.

$$\Phi_{\Delta}^{apparent} = g^{out} \times \Phi_{\Delta}^{S} \qquad (Eq.S12)$$

The two equations, S10 and S11, can be combined through the term k_{ox} yielding equation S13.

$$\frac{k_{PS}^{R}}{\Phi_{\Delta}^{R} \times I_{Abs}^{R} \times \tau_{\Delta}^{R}} = \frac{k_{PS}^{S}}{\Phi_{\Delta}^{apparent} \times I_{Abs}^{S} \times \tau_{\Delta}^{S}} \qquad (Eq.S13)$$

Rearranging and solving for the term $\Phi_{\Delta}^{apperent}$ yields equation S14.

$$\Phi_{\Delta}^{apparent} = \Phi_{\Delta}^{R} \times \frac{k_{PS}^{S}}{k_{PS}^{R}} \times \frac{I_{Abs}^{R}}{I_{Abs}^{S}} \times \frac{\tau_{\Delta}^{R}}{\tau_{\Delta}^{S}} \qquad (Eq.S14)$$

Under the identical conditions to those of PoP liposomes, indirect detection of singlet oxygen was performed on two reference photosensitizers in H_2O: Rose Bengal and Azure A. Two photosensitizers were chosen as references and were used independently in all of the $\Phi_{\Delta}^{apperent}$ calculations. This was done in order to test the agreement of the data, and to ensure the validity of the definition and the approach to calculation of $\Phi_{\Delta}^{apperent}$. Results of the indirect singlet oxygen detection experiments for Rose Bengal and Azure A reference photosensitizers are presented in figures S30 and S31. Values of Φ_{Δ}^{R} for photosensitizers in the presence and the absence of uric acid were obtained via direct detection which is described in the next section. Two photosensitizers were chosen as references and were used independently in all $\Phi_{\Delta}^{apperent}$ calculations to test the agreement of the data and to ensure the validity of the definition and the approach to the calculations. Final results of the indirect detection measurements are presented in table S8.

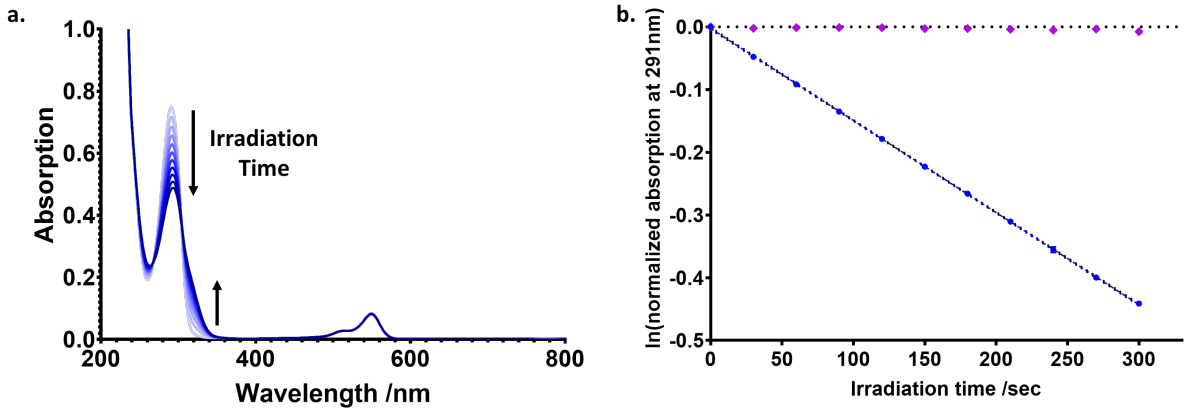

Figure S30: (a.) Singlet oxygen production from Rose Bengal in H_2O, as detected via the indirect detection methodology using uric acid (λ_{abs} = 291 nm) as the singlet oxygen sensitive probe. (b.) Evolution of uric acid absorption loss due to the selective irradiation of Rose Bengal under air equilibrated (blue spheres) and nitrogen purged (purple diamonds) conditions. Line of best-fit is shown as blue dotted line with a slope of $14.79 \pm 0.03 \times 10^{-4}$ s^{-1}. Data is based on duplicate measurements.

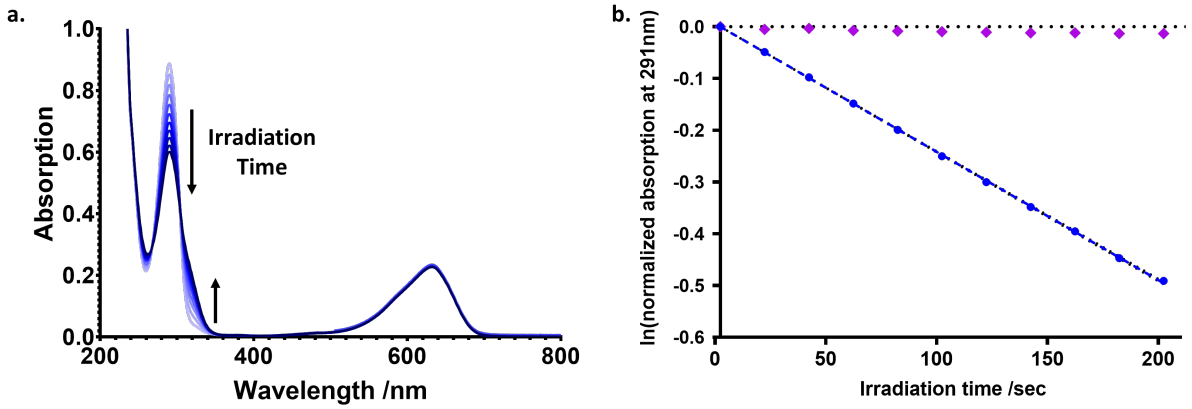

Figure S31: (a.) Singlet oxygen production from Azure A in H_2O, as detected via the indirect detection methodology using uric acid (λ_{abs} = 291 nm) as the singlet oxygen sensitive probe. (b.) Evolution of uric acid absorption loss due to the selective irradiation of Azure A under air equilibrated (blue spheres) and nitrogen purged (purple diamonds) conditions. Line of best-fit is shown as blue dotted line with a slope of $24.78 \pm 0.05 \times 10^{-4}$ s^{-1}. Data is based on duplicate measurements.

4.4 Assessment of photosensitizers' interactions with uric acid

Reference value for the quantum yield of singlet oxygen production of Azure A was obtained experimentally from the direct detection data (Figure S32 and table S5). Following equation 7 (main text) and using Rose Bengal as a reference (λ_{ex} = 532 nm; Φ_{Δ}^{R} = 0.75)[11], Azure A free in H_2O and excited at 532 nm was characterized to have Φ_{Δ} = 0.27 ± 0.02.

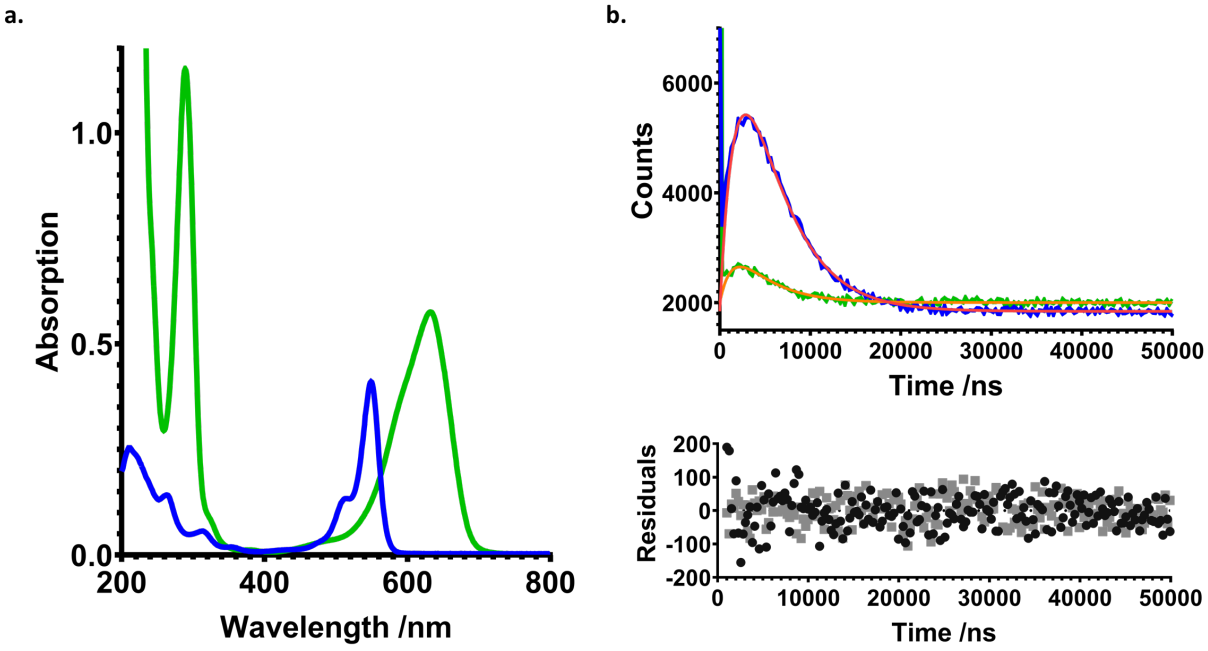

Figure S32: (a.) UV-Visible absorption spectra of Rose Bengal (blue) and Azure A (green) reference photosensitizers in water. (b.) Time-resolved $^1O_2$ phosphorescence signals at 1270 nm from the sample of Rose Bengal (blue) and the corresponding fit (red), and Azure A (green) and its corresponding fit (orange) obtained in H_2O. Residuals shown as black spheres are for fits to Rose Bengal sample, and grey squares are for fits to Azure A sample.

Table S5: Singlet oxygen phosphorescence decay curve fit parameters for Rose Bengal and Azure A samples in H_2O. [†]

	Rose Bengal	**Azure A**
S_0 /counts	6984 ± 111	1178 ± 82
τ_{Δ} /μs	4.3 ± 0.1	3.8 ± 0.3
$\tau_{triplet}$ /μs	2.00 ± 0.05	1.4 ± 0.2
Y_0 /counts	1843 ± 3	2003 ± 2

[†] Errors are based on the standard deviation of fitting equation S1 to the direct detection data

Importantly, uric acid has been previously reported to interfere with photosensitizers' abilities to produce singlet oxygen.[10] Therefore, we performed control experiment where singlet oxygen production was monitored via direct detection from both the references and the liposomes samples in the presence and the absence of uric acid (Figures S33 and S34, tables S6 and S7). As evident by the lack of statistically significant difference in the values of S_0 for any PoP liposome system with vs. without UA, it was concluded that uric acid had no significant effect on the ability of PoP liposomes to produce singlet oxygen. This result made sense as the porphyrin photosensitizer is encapsulated in the liposomal membrane which protects it from possible interactions with UA.[12] On the other hand, both Rose Bengal and Azure A had their singlet oxygen production abilities reduced in the presence of uric acid, which is consistent with the trends reported in the literature. Following equation 7 (main text), the quantum yields of these reference photosensitizers in the presence of uric acid (Φ_{Δ}^{R+UA}) were determined to be 0.66 ± 0.02 for Rose Bengal, and 0.21 ± 0.02 for Azure A. These reference values were used in further $\Phi_{\Delta}^{apperent}$ calculations.

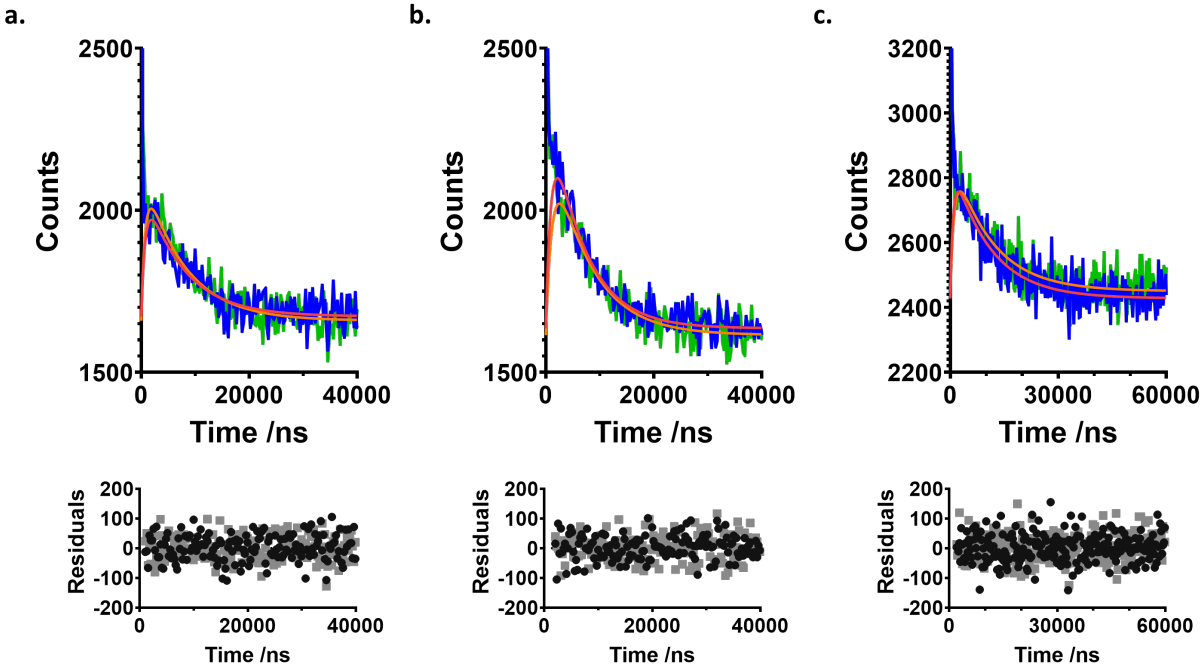

Figure S33: (a.) EMPTY PoP liposomes; (b.) DOX@PoP liposomes; (c.) IRT@PoP liposomes. Time-resolved $^1O_2$ phosphorescence signals at 1270 nm from the sample of PoP liposomes (blue) and the corresponding fit (red), and PoP liposomes in the presence of uric acid (green) and its corresponding fit (orange) obtained H_2O. Residuals shown as black spheres are for fits to PoP liposomes sample, and grey squares are for fits to PoP liposomes sample in the presence of uric acid.

Table S6: Singlet oxygen phosphorescence decay curve fit parameters for various PoP liposomes in the absence and presence of uric acid in H_2O. [†]

	Empty PoP	Empty PoP + Uric Acid	DOX@PoP	DOX@PoP + Uric Acid	IRT@PoP	IRT@PoP + Uric Acid
$S_0/counts$	391 ± 45	446 ± 44	661 ± 58	596 ± 66	409 ± 37	404 ± 44
$\tau_\Delta/\mu s$	7.3 ± 1.3	7.6 ± 1.2	6.8 ± 1.3	6.1 ± 1.2	10.5 ± 1.5	11.0 ± 2.0
$\tau_{triplet}/\mu s$	0.7 ± 0.2	0.7 ± 0.2	1.0 ± 0.2	1.1 ± 0.3	0.8 ± 0.4	1.1 ± 0.4
$Y_0/counts$	1673 ± 3	1659 ± 3	1636 ± 2	1615 ± 3	2428 ± 3	2450 ± 3

[†] Errors are based on the standard deviation of fitting equation S1 to the experimental data

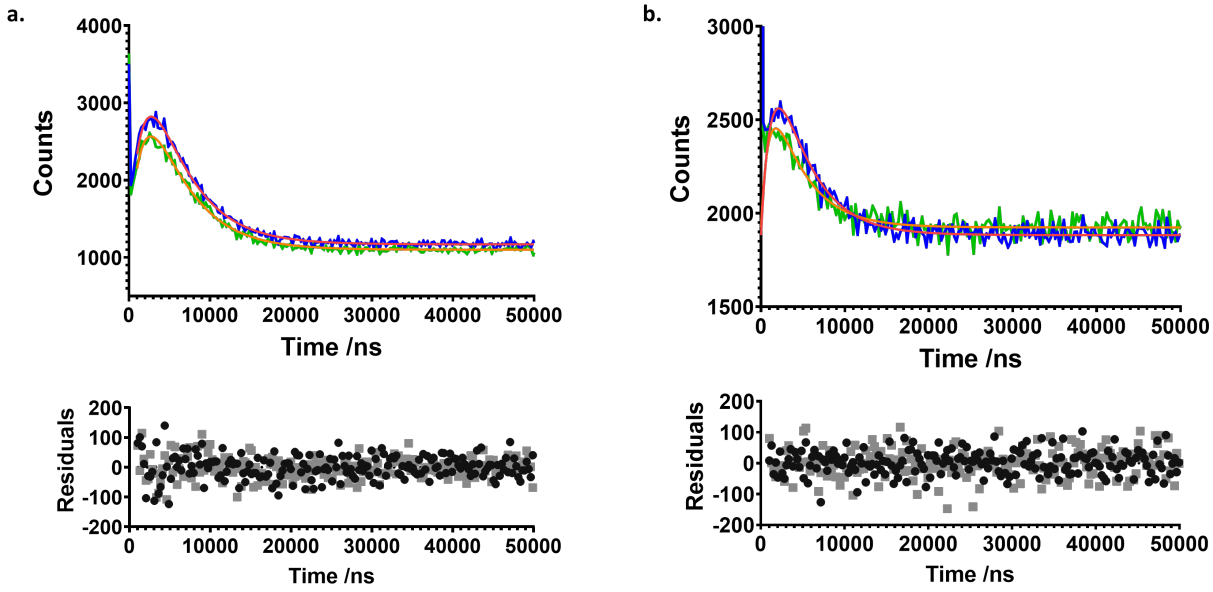

Figure S34: (a.) Rose Bengal; (b.) Azure A. Time-resolved $^1O_2$ phosphorescence signals at 1270 nm from the sample of reference photosensitizer (blue) and the corresponding fit (red), and reference photosensitizer in the presence of uric acid (green) and its corresponding fit (orange) obtained H_2O. Residuals shown as black spheres are for fits to reference photosensitizer sample, and grey squares are for fits to reference photosensitizer sample in the presence of uric acid.

Table S7: Singlet oxygen phosphorescence decay curve fit parameters for reference photosensitizers in the absence and presence of uric acid in H_2O. [†]

	Rose Bengal	**Rose Bengal + Uric Acid**	**Azure A**	**Azure A + Uric Acid**
S_0/*counts*	2943 ± 60	2585 ± 51	1137 ± 60	827 ± 54
τ_Δ/*μs*	4.7 ± 0.1	4.7 ± 0.1	4.1 ± 0.3	3.9 ± 0.3
$\tau_{triplet}$/*μs*	1.7 ± 0.6	1.7 ± 0.6	1.2 ± 0.1	0.9 ± 0.2
Y_0/*counts*	1169 ± 2	1100 ± 2	1883 ± 2	1924 ± 3

[†] Errors are based on the standard deviation of fitting equation S1 to the experimental data

Table S8: Singlet oxygen production quantum yields obtained via the indirect detection.

Reference System	*RB in the presence of UA* (Φ_Δ = 0.66 ± 0.02)	*AA in the presence of UA* (Φ_Δ = 0.21 ± 0.02)
EMPTY PoP [*]	0.13 ± 0.01	0.11 ± 0.01
DOX@PoP [*]	0.12 ± 0.01	0.11 ± 0.01
IRT@PoP [‡]	0.08 ± 0.01	0.07 ± 0.01

[*]Fully deconvoluted values for the porphyrin absorption were used in the calculations; [‡]Scattering deconvoluted values for the porphyrin + cargo absorption were used in the calculations.

4.5 Estimation of absolute singlet oxygen production quantum yield from IRT@PoP liposomes

Based on spectral deconvolution (table S1), at 355nm, 95% of all absorption for IRT@PoP samples is due to the IRT. Whereas, under the broadband irradiation conditions only 27% of total absorption is due to the drug (table S4). Given these absorption contribution values are known, the Φ_{Δ}^{direct} values of the empty PoP liposomes and of the free IRT can be used to estimate $\Phi_{\Delta}^{absolute}$ for IRT@PoP under the broadband irradiation conditions using equation S15.

$$\Phi_{\Delta}^{absolute-IRT@PoP} = \%\mathrm{I}_{\mathrm{Abs-IRT@PoP}}^{\mathrm{porphyrin}} \times \Phi_{\Delta}^{EMPTY\ PoP} + \%\mathrm{I}_{\mathrm{Abs-IRT@PoP}}^{\mathrm{cargo}} \times \Phi_{\Delta}^{free\ IRT} \qquad (Eq.S15)$$

It is important to note that equation S15 likely is an underestimation of true $\Phi_{\Delta}^{absolute}$ value for IRT@PoP liposomes, as it does not account for any possible inner-filter effect potentially occurring between the encapsulated IRT drug and the membrane porphyrin (speculated to occur basedo n the overlap of emission of IRT and absorption of the porphyrin). Exploring the nature of the latter is beyond the scope of this study. However, under broadband irradiation conditions most of the integrated absorption is due to the porphyrin (table S4), thus we believe the error associated with not accounting for the aforementioned effect is minimal. Following the data obtained in sections 4.2 and 4.5, $\Phi_{\Delta}^{absolute}$ for IRT@PoP liposomes can be estimated to equal 0.53 ± 0.04.

4.6 Fractions of singlet oxygen lifetime spent in the inner- and membrane- liposomal environments

We assume that deuterated solvent will not have an effect of the rate of singlet oxygen deactivation within the lipid membrane. Further assuming equilibrium conditions between the solvent environment outside and inside of the liposomes, equation S2 can be rewritten as equations S16 and S17 for samples in H_2O and 95% D_2O, respectively.

$$k_{H_2O}^{obs} = g^{out}k_{H_2O}^{out} + g^{lipid}k^{lipid} + g^{in}k_{H_2O}^{in} \qquad (Eq.S16)$$

$$k_{D_2O}^{obs} = g^{out}k_{D_2O}^{out} + g^{lipid}k^{lipid} + g^{in}k_{D_2O}^{in} \qquad (Eq.S17)$$

Notably, the values of g^{out} and k^{out} in both solvents are known (section 4.6), these variables can therefore be combined with the observed rates of singlet oxygen deactivation (k^{obs}). Furthermore, keeping the relationship between the values of g in mind (equation S3), equations S16 and S17 can be rewritten in the form of equations S18 and S19.

$$k_{H_2O}^{obs} - g^{out}k_{H_2O}^{out} = g^{lipid}k^{lipid} + \left(1 - g^{out} - g^{lipid}\right)k_{H_2O}^{in} \qquad (Eq.S18)$$

$$k_{D_2O}^{obs} - g^{out}k_{D_2O}^{out} = g^{lipid}k^{lipid} + \left(1 - g^{out} - g^{lipid}\right)k_{D_2O}^{in} \qquad (Eq.S19)$$

Expanding equations S18 and S19, yields equations S20 and S21.

$$k_{H_2O}^{obs} - g^{out}k_{H_2O}^{out} = g^{lipid}k^{lipid} + k_{H_2O}^{in} - g^{out}k_{H_2O}^{in} - g^{lipid}k_{H_2O}^{in} \qquad (Eq.S20)$$

$$k_{D_2O}^{obs} - g^{out}k_{D_2O}^{out} = g^{lipid}k^{lipid} + k_{D_2O}^{in} - g^{out}k_{D_2O}^{in} - g^{lipid}k_{D_2O}^{in} \qquad (Eq.S21)$$

Rearranging for the value of g^{lipid}, gives equations S22 and S23, which can consequently be combined in equation S24.

$$\frac{k_{H_2O}^{obs} - g^{out}k_{H_2O}^{out} - k_{H_2O}^{in} + g^{out}k_{H_2O}^{in}}{k^{lipid} - k_{H_2O}^{in}} = g^{lipid} \qquad (Eq.S22)$$

$$\frac{k_{D_2O}^{obs} - g^{out}k_{D_2O}^{out} - k_{D_2O}^{in} + g^{out}k_{D_2O}^{in}}{k^{lipid} - k_{D_2O}^{in}} = g^{lipid} \qquad (Eq.S23)$$

$$\frac{k_{H_2O}^{obs} - g^{out}k_{H_2O}^{out} - k_{H_2O}^{in} + g^{out}k_{H_2O}^{in}}{k^{lipid} - k_{H_2O}^{in}} = \frac{k_{D_2O}^{obs} - g^{out}k_{D_2O}^{out} - k_{D_2O}^{in} + g^{out}k_{D_2O}^{in}}{k^{lipid} - k_{D_2O}^{in}} \qquad (Eq.S24)$$

Using equation S24, the value of k^{lipid} can be found through several steps. For clarity, equations S22 and S23 can first be introduced, where values of *A* and *B* can be calculated using the experimentally obtained quantities from the previous sections.

$$k_{H_2O}^{obs} - g^{out}k_{H_2O}^{out} - k_{H_2O}^{in} + g^{out}k_{H_2O}^{in} = A \qquad (Eq.S25)$$

$$k_{D_2O}^{obs} - g^{out}k_{D_2O}^{out} - k_{D_2O}^{in} + g^{out}k_{D_2O}^{in} = B \qquad (Eq.S26)$$

Equation S24, can then be rewritten and transformed into the form of equation S27.

$$A \times \left(k^{lipid} - k_{D_2O}^{in}\right) = B \times \left(k^{lipid} - k_{H_2O}^{in}\right) \qquad (Eq.S27)$$

Solving for the value of k^{lipid}, yields equation S28.

$$\frac{B \times k_{H_2O}^{in} - A \times k_{D_2O}^{in}}{B - A} = k^{lipid} \qquad (Eq.S28)$$

4.7 Liposome encapsulated drugs degradation due to laser irradiation

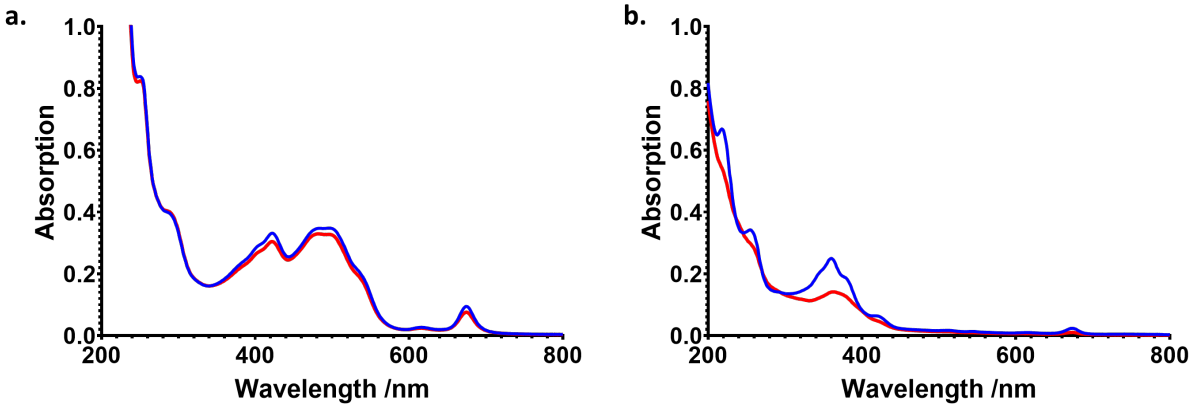

Figure S35: UV-Visible spectra for (a.) DOX@PoP liposomes and (b.) IRT@PoP liposomes in H_2O before (blue) and after (red) 10 minutes of laser irradiation at 355nm.

References

1. K. A. Carter, S. Shao, M. I. Hoopes, D. Luo, B. Ahsan, V. M. Grigoryants, W. Song, H. Huang, G. Zhang, R. K. Pandey, J. Geng, B. A. Pfeifer, C. P. Scholes, J. Ortega, M. Karttunen and J. F. Lovell, *Nat Commun*, 2014, **5**, 3546.
2. D. Luo, K. A. Carter, A. Razi, J. Geng, S. Shao, D. Giraldo, U. Sunar, J. Ortega and J. F. Lovell, *Biomaterials*, 2016, **75**, 193-202.
3. D. C. Drummond, C. O. Noble, Z. Guo, K. Hong, J. W. Park and D. B. Kirpotin, *Cancer Research,* 2006, **66**, 3271-3277.
4. N. Macia, V. Kabanov, M. Côté-Cyr and B. Heyne, *The Journal of Physical Chemistry Letters*, 2019, **10**, 3654-3660.
5. K. Nawara, P. Krysinski and G. J. Blanchard, *The Journal of Physical Chemistry A*, 2012, **116**, 4330-4337.
6. S. Nonell and S. E. Braslavsky, in *Methods in Enzymology*, Academic Press, 2000, vol. 319, pp. 37-49.
7. J. R. Hurst and G. B. Schuster, *Journal of the American Chemical Society*, 1983, **105**, 5756-5760.
8. R. Schmidt and H. D. Brauer, *Journal of the American Chemical Society*, 1987, **109**, 6976-6981.
9. G. Boso, D. Ke, B. Korzh, J. Bouilloux, N. Lange and H. Zbinden, *Biomedical Optics Express*, 2016, **7**, 211-224.
10. M. Bregnhøj, L. Dichmann, C. K. McLoughlin, M. Westberg and P. R. Ogilby, *Photochemistry and Photobiology*, 2019, **95**, 202-210.
11. F. Wilkinson, W. P. Helman and A. B. Ross, *Journal of Physical and Chemical Reference Data*, 1993, **22**, 113-262.
12. I. Noiseux, O. Mermut, J.-P. Bouchard, J.-F. Cormier, P. Desroches, M. Fortin, P. Gallant, S. Leclair, M. Vernon, K. R Diamond and M. S Patterson, *Journal of Biomedical Optics*, 2008, **13**, 041313.